POLITECNICO DI TORINO
Repository ISTITUZIONALE

Studies of J/ production at forward rapidity in Pb–Pb collisions at sNN = 5.02 TeV

Original
Studies of J/ production at forward rapidity in Pb–Pb collisions at sNN = 5.02 TeV / Acharya, S., Adamova, D., Adolfson, J., Aggarwal, M., Rinella, G., Agnello, M., Agrawal, N., Bufalino, S., Concas, M., Grosa, F., Ravasenga, I., Fecchio, P., Catalano, F.. - In: JOURNAL OF HIGH ENERGY PHYSICS. - ISSN 1029-8479. - STAMPA. - 2020:2(2020), p. 041. [10.1007/JHEP02(2020)041]

Availability:
This version is available at: 11583/2848773 since: 2020-10-16T10:45:47Z

Publisher:
Springer

Published
DOI:10.1007/JHEP02(2020)041

Terms of use:

This article is made available under terms and conditions as specified in the corresponding bibliographic description in the repository

Publisher copyright
Springer postprint/Author's Accepted Manuscript

This version of the article has been accepted for publication, after peer review (when applicable) and is subject to Springer Nature's AM terms of use, but is not the Version of Record and does not reflect post-acceptance improvements, or any corrections. The Version of Record is available online at: http://dx.doi.org/10.1007/JHEP02(2020)041

(Article begins on next page)

19 November 2026

Published for SISSA by Springer

Received: October 18, 2019
Accepted: January 15, 2020
Published: February 6, 2020

Studies of J/ψ production at forward rapidity in Pb–Pb collisions at $\sqrt{s_{\rm NN}} = 5.02$ TeV



The ALICE collaboration

E-mail: ALICE-publications@cern.ch

Abstract: The inclusive J/ψ production in Pb–Pb collisions at the center-of-mass energy per nucleon pair $\sqrt{s_{\rm NN}} = 5.02$ TeV, measured with the ALICE detector at the CERN LHC, is reported. The J/ψ meson is reconstructed via the dimuon decay channel at forward rapidity ($2.5 < y < 4$) down to zero transverse momentum. The suppression of the J/ψ yield in Pb–Pb collisions with respect to binary-scaled pp collisions is quantified by the nuclear modification factor ($R_{\rm AA}$). The $R_{\rm AA}$ at $\sqrt{s_{\rm NN}} = 5.02$ TeV is presented and compared with previous measurements at $\sqrt{s_{\rm NN}} = 2.76$ TeV as a function of the centrality of the collision, and of the J/ψ transverse momentum and rapidity. The inclusive J/ψ $R_{\rm AA}$ shows a suppression increasing toward higher transverse momentum, with a steeper dependence for central collisions. The modification of the J/ψ average transverse momentum and average squared transverse momentum is also studied. Comparisons with the results of models based on a transport equation and on statistical hadronization are carried out.

Keywords: Hadron-Hadron scattering (experiments)

ArXiv ePrint: 1909.03158

Open Access, Copyright CERN,
for the benefit of the ALICE Collaboration.
Article funded by SCOAP^3.

https://doi.org/10.1007/JHEP02(2020)041

JHEP02(2020)041

Contents

1 Introduction 1

2 Apparatus and data sample 2

3 Data analysis 4

4 Results 7

4.1 Nuclear modification factor 7

4.1.1 Centrality-integrated $R_{\rm AA}$ as a function of y and $p_{\rm T}$ 8

4.1.2 Centrality-differential $R_{\rm AA}$ as a function of y and $p_{\rm T}$ 8

4.1.3 Centrality dependence of $R_{\rm AA}$ 10

4.2 J/ψ average transverse momentum and $r_{\rm AA}$ 13

5 Conclusions 16

The ALICE collaboration 23

1 Introduction

The study of ultra-relativistic heavy-ion collisions aims to investigate the properties of strongly-interacting matter at high temperature and energy density. Lattice Quantum Chromodynamics calculations predict that a deconfined state of partonic matter, the so-called Quark–Gluon Plasma (QGP), can be created in such collisions [1–3]. Among the many possible probes to study this phase of matter, heavy quarks (charm (c) and beauty (b)) are particularly interesting as they are expected to be produced in the initial stage of the collisions, by hard partonic scatterings, and to experience the full evolution of the system. In particular, it was predicted that bound states of c and $\overline{\rm c}$ quarks (known as charmonia) should be suppressed due to the color-screening mechanism [4]. The suppression probabilities of the quarkonium ($\rm c\overline{c}$ or $\rm b\overline{b}$) states in the QGP depend on their binding energies and the medium temperature. Therefore, the measurement of the relative production rates of the quarkonium states should give indications on the temperature of the system [5]. Among the different charmonium states, the study of the ground state with quantum numbers $J^{PC} = 1^{--}$ (J/ψ) is comparatively more accessible due to its larger abundance and to the relatively large branching ratio to dileptons, and has led to several important results.

Over the past decades, the J/ψ production in heavy-ion collisions was measured at the SPS, RHIC and the LHC, covering a wide range of center-of-mass energies per nucleon pair ($\sqrt{s_{\rm NN}}$) from about 17 GeV to 5.02 TeV. A suppression of the J/ψ production yield in nucleus–nucleus (AA) relative to that expected from measurements in proton–proton (pp) collisions was observed at the SPS at $\sqrt{s_{\rm NN}} = 17$ GeV [6, 7], at RHIC up to

JHEP02(2020)041

$\sqrt{s_{\rm NN}} = 0.2\,\text{TeV}$ [8–11] and at the LHC at $\sqrt{s_{\rm NN}} = 2.76\,\text{TeV}$ [12–16] and 5.02 TeV [17–19]. The suppression is evaluated through the calculation of the nuclear modification factor ($R_{\rm AA}$), corresponding to the ratio of the production yields in AA and the cross section in pp collisions, normalised by the nuclear overlap function ($\langle T_{\rm AA}\rangle$) [20]. The observed suppression does not increase with increasing collision energy as expected in the color-screening picture considering the increasing temperature of the formed QGP. This observation is naturally explained by a further production mechanism known as regeneration, in which abundantly produced $\rm c\overline{c}$ pairs recombine into J/ψ [21, 22]. The contribution of the regeneration to J/ψ production has to increase with the density of $\rm c\overline{c}$ pairs and consequently with the collision energy. It is worth noting that the regeneration contribution should favour low transverse momentum ($p_{\rm T}$) J/ψ, as the bulk of charm quarks are produced at small momenta [21, 22]. The regeneration scenario was further supported by the measurement of a positive J/ψ elliptic flow (v_2) [23–27] which, at low $p_{\rm T}$, can be acquired via charm-quark recombination [28, 29]. It is important to note that in addition to the effects discussed above, related to the production of a high energy-density medium, the so-called cold-nuclear-matter effects may also have a sizeable influence on the charmonium yields. In particular, the modification of the parton distribution functions in the nucleus (e.g. nuclear shadowing [30, 31]) may modify the initial yields of charm quarks and has to be taken into account in the interpretation of the results. Quantitative estimates of these effects are carried out via the study of proton–nucleus collisions [32–37]. Finally, a quantitative interpretation of the results requires taking into account that the observed J/ψ are produced either promptly, i.e. as direct J/ψ or via decay of higher-mass charmonium states ($\chi_{\rm c}$, $\psi(2S)$), or non-promptly through the weak decay of hadrons containing a b quark [38].

For a better assessment of the suppression-regeneration scenario, extensive studies of the centrality, $p_{\rm T}$ and rapidity dependence of the J/ψ nuclear modification factor have to be carried out. The first ALICE measurement of the inclusive (sum of prompt and non-prompt sources) J/ψ production at $\sqrt{s_{\rm NN}} = 5.02\,\text{TeV}$ at forward rapidity [17] has shown a hint for an increase of $R_{\rm AA}$ with respect to the $\sqrt{s_{\rm NN}} = 2.76\,\text{TeV}$ results in the region $2 < p_{\rm T} < 6\,\text{GeV}/c$, while the results were consistent elsewhere.

In this paper, we complement the results obtained in ref. [17]. The J/ψ $R_{\rm AA}$ is simultaneously obtained in different collision centrality classes and $p_{\rm T}$ or rapidity intervals. In addition, to further assess the kinematic region of influence of the J/ψ regeneration mechanism, results on the J/ψ average $p_{\rm T}$ and $p_{\rm T}^2$ as a function of centrality are presented.

The paper is organized as follows: section 2 is dedicated to the description of the ALICE detector systems used in this analysis. The analysis procedure is briefly explained and a summary of the systematic uncertainties is also given in section 3. Results are presented and compared to available measurements at $\sqrt{s_{\rm NN}} = 2.76\,\text{TeV}$ and model calculations in section 4.

2 Apparatus and data sample

The ALICE detector and its performance are extensively described in refs. [39] and [40], respectively. J/ψ mesons are reconstructed in the muon spectrometer (covering the pseudo-

JHEP02(2020)041

rapidity interval $-4 < \eta < -2.5$[1]) via their dimuon decay channel down to zero p_{T}. The muon spectrometer consists of a 4.1 m (10 interaction lengths (λ_{int})) thick front absorber which is used to filter out hadrons coming from the interaction point (IP), followed by tracking (MCH) and triggering (MTR) systems. Each of the five tracking stations is composed of two planes of cathode pad chambers. The third tracking station is located inside a dipole magnet with a field integral of 3 Tm. A 1.2 m ($7.2\lambda_{\mathrm{int}}$) thick iron wall, which absorbs secondary hadrons escaping from the front absorber and low-momentum muons produced predominantly from π and K decays, is located between the tracking system and the trigger stations. Each of the two trigger stations consists of two planes of resistive plate chambers. Finally, a small-angle conical absorber around the beam-pipe protects the spectrometer from secondary particles produced by interactions of large-η primary particles with the beam-pipe.

The other detectors used in this analysis are the Silicon Pixel Detector (SPD), the V0 scintillator detectors, the Cherenkov detectors T0 and the Zero Degree Calorimeters (ZDC). The SPD [41] provides the coordinates of the primary vertex of the collision, and consists of two cylindrical layers covering $|\eta| < 2$ (inner layer) and $|\eta| < 1.4$ (outer layer). The V0 [42], composed of two arrays of 32 scintillator tiles each, and located on both sides of the IP, covers $2.8 < \eta < 5.1$ (V0A) and $-3.7 < \eta < -1.7$ (V0C), and is used as a trigger detector, for the centrality determination and to remove beam-induced background. It is also used for the measurement of the luminosity along with the T0 detector [43], which consists of two quartz Cherenkov counters, located on each side of the IP and covering the pseudo-rapidity intervals $-3.3 < \eta < -3$ and $4.6 < \eta < 4.9$. The ZDCs, located on either side of the IP at $\pm$ 114 m along the beam axis, detect spectator nucleons emitted at zero degrees with respect to the LHC beam axis, and are used to reject electromagnetic Pb–Pb interactions [44].

The centrality determination and the evaluation of the average number of participant nucleons in the collision ($\langle N_{\mathrm{part}} \rangle$) for each centrality class is based on a Glauber model fit to the V0 signal amplitude distribution as described in refs. [45, 46]. The events are classified in centrality classes corresponding to percentiles of the nuclear hadronic cross section. In this analysis, events corresponding to the most central 90% of the inelastic cross section were selected. For these events the minimum bias (MB) trigger is fully efficient and the residual contamination from electromagnetic processes is negligible. The MB trigger is defined by a coincidence of the signals from both sides of the V0 detector.

The analysis presented here is based on dimuon-triggered events which require, in addition to the MB condition, the detection of two Unlike-Sign (US) tracks in the triggering system of the muon spectrometer. The muon trigger selects muon candidates having a transverse momentum larger than a given threshold which corresponds to the value for which the trigger efficiency reaches 50%. In Pb–Pb collisions the p_{T} threshold is $\approx 1\,\mathrm{GeV}/c$ with the single-muon trigger efficiency reaching a plateau value of 98% at $\approx 2.5\,\mathrm{GeV}/c$ [47].

The current analysis exploits the data samples of Pb–Pb collisions at $\sqrt{s_{\mathrm{NN}}} = 5.02\,\mathrm{TeV}$ collected during 2015. This corresponds to an integrated luminosity $L_{\mathrm{int}}^{\mathrm{PbPb}} \approx 225\ \mu\mathrm{b}^{-1}$.

[1] In the ALICE reference frame, the muon spectrometer covers a negative η interval and consequently negative y values. We have chosen to present our results with a positive y notation.

JHEP02(2020)041

3 Data analysis

For a centrality class i, the double-differential J/ψ invariant yield ($Y^i_{\mathrm{J}/\psi}$) is defined as

$$\frac{\mathrm{d}^2 Y^i_{\mathrm{J}/\psi}}{\mathrm{d}y\mathrm{d}p_{\mathrm{T}}} = \frac{N^i_{\mathrm{J}/\psi}(p_{\mathrm{T}}, y)}{\mathrm{BR}_{\mathrm{J}/\psi\to\mu^+\mu^-} \cdot \Delta p_{\mathrm{T}} \cdot \Delta y \cdot (A \times \varepsilon)^i(p_{\mathrm{T}}, y) \cdot N^i_{\mathrm{MB}}}, \tag{3.1}$$

where $N^i_{\mathrm{J}/\psi}(p_{\mathrm{T}}, y)$ is the number of J/ψ for a given p_{T} and y interval, $\mathrm{BR}_{\mathrm{J}/\psi\to\mu^+\mu^-} = (5.96 \pm 0.03)\%$ is the branching ratio of the dimuon decay channel [48], Δp_{T} and Δy are respectively the widths of the p_{T} and y intervals, $(A \times \varepsilon)^i(p_{\mathrm{T}}, y)$ is the product of the detector acceptance and the reconstruction efficiency for that p_{T} and y interval, and N^i_{MB} is the equivalent number of minimum-bias events. The values of N^i_{MB} are obtained as the product of the number of dimuon-triggered events times the inverse of the probability of having a dimuon trigger in a MB event (F^i). The F^i values correspond to those quoted in ref. [17]. For the centrality integrated sample, the value of the normalization factor is $F^{0-90\%} = 11.84 \pm 0.06$. The quoted uncertainty is systematic and corresponds to the difference between the results obtained with two methods, either by calculating the ratio of the counting rates of the two triggers, or by applying the dimuon trigger condition in the analysis of MB events.

The nuclear modification factor R_{AA} is given by

$$R^i_{\mathrm{AA}}(p_{\mathrm{T}}, y) = \frac{\mathrm{d}^2 Y^i_{\mathrm{J}/\psi}/\mathrm{d}y\mathrm{d}p_{\mathrm{T}}}{\langle T_{\mathrm{AA}}\rangle^i \cdot \mathrm{d}^2\sigma^{\mathrm{pp}}_{\mathrm{J}/\psi}/\mathrm{d}y\mathrm{d}p_{\mathrm{T}}}, \tag{3.2}$$

where $\langle T_{\mathrm{AA}}\rangle^i$ is the average of the nuclear-overlap function [20]. The values of $\langle T_{\mathrm{AA}}\rangle^i$ in different centrality classes were obtained using a Glauber calculation [46, 49, 50]. The systematic uncertainty on the $\langle T_{\mathrm{AA}}\rangle^i$ calculation, which ranges from 1% in the most central class to 3% in the most peripheral one, was determined by varying the density parameters of the Pb nucleus and the nucleon–nucleon inelastic cross section within their uncertainties. The systematic uncertainty on the definition of the centrality intervals is evaluated by varying by $\pm 0.5\%$ the fraction (90%) of the hadronic cross section selected with the chosen minimal cut on the V0 signal amplitude, and redefining accordingly the centrality intervals, following the approach detailed in ref. [17]. Values of the J/ψ cross section in pp collisions ($\mathrm{d}^2\sigma^{\mathrm{pp}}_{\mathrm{J}/\psi}/\mathrm{d}y\mathrm{d}p_{\mathrm{T}}$) at $\sqrt{s} = 5.02\,\mathrm{TeV}$ were already reported in refs. [17, 51] and are used here as a reference. In addition, following the same analysis procedure as detailed in those papers, the cross section was evaluated in four p_{T} intervals (0.3–2, 2–5, 5–8, and 8–12 GeV/c) for the interval $2.5 < y < 4$ and three y intervals (2.5–3, 3–3.5, and 3.5–4) for the interval $p_{\mathrm{T}} < 12\,\mathrm{GeV}/c$. The integrated luminosity of the pp sample is $L^{\mathrm{pp}}_{\mathrm{int}} = (106.3 \pm 2.2)\,\mathrm{nb}^{-1}$ [52].

The J/ψ candidates were formed by combining US muons reconstructed within the geometrical acceptance of the muon spectrometer using the tracking algorithm described in ref. [53]. The selection criteria applied to both single muons and dimuons are identical to the ones used in refs. [14, 17], requiring a match between tracks reconstructed in the tracking system and track segments in the muon trigger system.

JHEP02(2020)041

The signal extraction was performed over the US dimuon invariant mass ranges [2.2,4.5] and [2.4,4.7] GeV/c^2 using two methods. In the first one, the invariant mass distributions were fitted with the sum of a signal and a background function. In the second one, the combinatorial background (dominant in central Pb–Pb collisions) was first estimated using an event-mixing technique [14], and then subtracted from the raw invariant mass distribution. Finally, the resulting distributions were fitted with the sum of a signal and a residual background component.

The signal component of the fitting function is either a double-sided Crystal Ball function (CB2, where independent non-Gaussian tails are present on both sides of a Gaussian core) or a pseudo-Gaussian with a mass-dependent width [54]. For both functions, the position of the J/ψ pole mass, as well as the width of the resonance, are free parameters of the fits, while the non-Gaussian tail parameters were fixed. Two sets of tail parameters were obtained from Monte Carlo (MC) simulations using different particle transport codes (GEANT3 [55] and GEANT4 [56]) to account for the sensitivity of these parameters to the description of the detector materials. In addition, another set of CB2 tail parameters was extracted from the pp collisions at $\sqrt{s} = 13$ TeV data sample [51], the sample with the largest significance of the J/ψ signal. The ψ(2S) signal was included in the fits using the same signal functions as for the J/ψ, with mass and width tied to those of the J/ψ [57].

The background was parametrized either as a pseudo-Gaussian with a width quadratically dependent on the mass or as a ratio of a 2$^{\text{nd}}$ to 3$^{\text{rd}}$ order polynomial. When using the event-mixing technique, the continuum component of the correlated background remaining in the US dimuon distributions after the background subtraction and originating mainly from semi-muonic decays of pairs of charm hadrons, was parametrized using the sum of two exponential functions. Examples of fits to the US dimuon invariant mass distributions, without and with subtraction of mixed-event background, are shown in figure 1 for different centrality classes and p_{T} intervals. For each centrality class, p_{T} and y interval, the number of J/ψ and the statistical uncertainty are given by the average of the results from the considered fit configurations obtained by varying the signal and background functions, the tail parameters and the invariant mass fit range. The systematic uncertainty is defined, for each centrality, p_{T} and y interval, as the RMS of the various fit results. It varies between 1.5% and 3.6% as a function of centrality or p_{T} and between 1.5% and 5% as a function of y.

The J/ψ $A \times \varepsilon$ was obtained using MC simulations, where the p_{T} and y distributions for the generated J/ψ were matched to the ones extracted from data using an iterative procedure as done in ref. [33]. Unpolarized J/ψ production was assumed, consistently with the measurements of inclusive J/ψ polarization in pp collisions [58, 59]. The misalignment of the detection elements as well as the time-dependent status of each electronic channel during the data taking period were taken into account in the simulation. Generated J/$\psi \to \mu^+\mu^-$ signals were embedded into real minimum bias events in order to properly reproduce the effect of detector occupancy and its variation from one centrality class to another, and reconstructed as for real events. A relative decrease by ∼14% of $A \times \varepsilon$ was observed in the most central Pb–Pb collisions with respect to the most peripheral ones.

The following sources of systematic uncertainty on $A \times \varepsilon$ were considered: (i) the parametrization of the input p_{T} and y shapes, (ii) the uncertainty on the tracking efficiency

JHEP02(2020)041

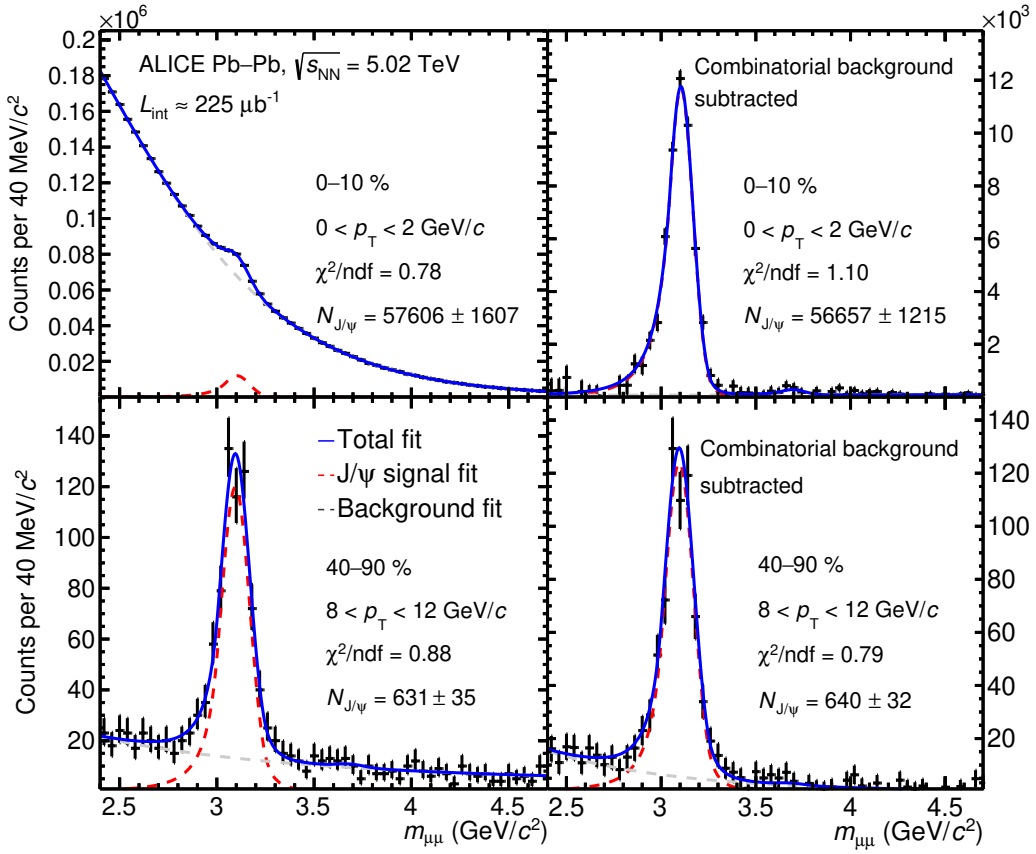


Figure 1. Example of fits to the US dimuon invariant mass distributions in Pb–Pb collisions at $\sqrt{s_{\rm NN}} = 5.02\,\text{TeV}$ in different centrality classes and $p_{\rm T}$ intervals. The left (right) panels show the distributions before (after) background subtraction with the event-mixing technique. Dashed gray curves correspond to background functions, red curves to the signal functions and blue curves to the sum of the signal and background functions.

in the muon tracking chambers, (iii) the uncertainty on the MTR efficiency and (iv) the matching between tracks reconstructed in the tracking and triggering systems.

For the parametrization of the MC input distributions, two sources of systematic uncertainty were considered: the effect of the finite data sample used to parametrize these distributions and the correlations between $p_{\rm T}$ and y (more explicitly, the fact that the $p_{\rm T}$ distribution of the J/ψ varies within the rapidity interval in which it is measured). The former turns out to be negligible. For the latter, different MC simulations were performed by varying the input $p_{\rm T}$ and y distributions within limits that correspond to this effect and re-calculating the $A \times \varepsilon$ in each case as done in ref. [51]. The uncertainties on the tracking efficiency in the MCH, trigger efficiency in the MTR, and on the matching efficiency between MTR and MCH tracks were evaluated by comparing the efficiencies obtained in data and MC at the single muon level and propagating the observed differences to the J/ψ candidates, as done in ref. [60].

In each centrality, $p_{\rm T}$ and y interval, the total systematic uncertainty on the yield and $R_{\rm AA}$ is determined as the quadratic sum of the uncertainties from the different sources listed

JHEP02(2020)041

Sources	vs centrality	vs p_{T}	vs y
Signal extraction	1.5–3.6	1.5–3.6	1.5–5.0
MC input	2*	2–3	0.5–2.5
Tracking efficiency	3*	3	3
Trigger efficiency	1.5–2.7 *	1.5–4.1	1.5–2.4
Matching efficiency	1*	1	1
F	0.5*	0.5*	0.5*
BR (only on yield) [48]	0.5*	0.5*	0.5*
$\langle T_{\mathrm{AA}} \rangle$ (only on R_{AA})	0.7–3.2	0.7–2.0*	0.7–2.0*
Centrality definition	0.1–3.5	0.2–1.4*	0.2–1.4*
pp reference (only on R_{AA})	4.9–10.9*	4.4–16.5 and 2.1*	4.7–8.5 and 2.1*

Table 1. Summary of systematic uncertainties, in percentage, on the yield and R_{AA} in Pb–Pb collisions at $\sqrt{s_{\mathrm{NN}}} = 5.02\,\mathrm{TeV}$. Values with an asterisk correspond to the systematic uncertainties correlated as a function of the given variable. For the pp reference, the correlated and uncorrelated contributions are separated.

in table 1. Correlations of various uncertainties vs centrality, p_{T} or y are also reported. The values in the last row correspond to the sum of the statistical and systematic uncertainties on the pp reference.

4 Results

4.1 Nuclear modification factor

This section summarizes the results for the inclusive J/ψ R_{AA} at forward rapidity in Pb–Pb collisions at $\sqrt{s_{\mathrm{NN}}} = 5.02\,\mathrm{TeV}$ as a function of:

- rapidity and transverse momentum, integrated over the centrality (class 0–90%);
- rapidity and transverse momentum, for the centrality classes 0–20%, 20–40% and 40–90%;
- centrality, in four transverse momentum intervals and in three rapidity intervals.

When possible, the ratio between the results of this analysis and the measurements in Pb–Pb collisions at $\sqrt{s_{\mathrm{NN}}} = 2.76\,\mathrm{TeV}$ [14], in the same kinematic interval, is computed. Only the uncertainty related to the $\langle T_{\mathrm{AA}} \rangle$ cancels out in the ratio, as discussed in ref. [17]. Following the same approach as in refs. [14, 17], an estimate of the R_{AA} of prompt J/ψ was determined by making conservative assumptions on the size of the non-prompt R_{AA}. The relation between the inclusive (R_{AA}), prompt ($R_{\mathrm{AA}}^{\mathrm{prompt}}$) and non-prompt ($R_{\mathrm{AA}}^{\mathrm{non\text{-}prompt}}$) nuclear modification factors can be expressed as:

$$R_{\mathrm{AA}}^{\mathrm{prompt}} = \frac{R_{\mathrm{AA}} - F_{\mathrm{B}} \cdot R_{\mathrm{AA}}^{\mathrm{non\text{-}prompt}}}{1 - F_{\mathrm{B}}}, \tag{4.1}$$

JHEP02(2020)041

where $F_{\rm B}$ is the fraction of non-prompt to inclusive J/ψ in pp collisions. This quantity is evaluated at $\sqrt{s} = 5.02\,\text{TeV}$ by interpolating in energy the corresponding LHCb cross-section measurements in pp collisions at $\sqrt{s} = 2.76$ and 7 TeV [61–63]. The limits on $R_{\rm AA}^{\rm prompt}$ correspond to the two extreme hypotheses of total non-prompt J/ψ suppression ($R_{\rm AA}^{\text{non-prompt}} = 0$) and absence of suppression ($R_{\rm AA}^{\text{non-prompt}} = 1$). The effect is small at moderate transverse momentum ($\lesssim 10\%$ for $p_{\rm T} \lesssim 5\,\text{GeV}/c$) and then increases at higher $p_{\rm T}$. Numerical values for the limits on $R_{\rm AA}^{\rm prompt}$ can be found in the HepData record associated to this paper. Another effect which may influence the interpretation of the inclusive J/ψ results is the presence of an excess at very low $p_{\rm T}$, observed at $\sqrt{s_{\rm NN}} = 2.76\,\text{TeV}$ [64] and related to J/ψ photo-production [65]. This source was shown to be significant with respect to hadronic production for peripheral Pb–Pb collisions and has a strong influence on the measured $R_{\rm AA}$ values. For this reason, the region $p_{\rm T} < 0.3\,\text{GeV}/c$ was excluded when dealing with peripheral collisions. The remaining contribution of this source to the region $p_{\rm T} > 0.3\,\text{GeV}/c$ was evaluated following the procedure detailed in ref. [14] and the maximum effect on $R_{\rm AA}$ is explicitly shown in the following figures by use of bracket symbols. The upper and lower limit brackets correspond to the extremest hypotheses on the contribution from photo-produced J/ψ and on the efficiency of the aforementioned $p_{\rm T}$ selection as described in ref. [14].

4.1.1 Centrality-integrated $R_{\rm AA}$ as a function of y and $p_{\rm t}$

Figures 2 and 3 show the inclusive J/ψ nuclear modification factor as a function of transverse momentum and rapidity, integrated over the centrality class 0–90%. The results are compared with those obtained at $\sqrt{s_{\rm NN}} = 2.76\,\text{TeV}$ [14] and with the results of the calculation of a transport model [28, 66]. A significant increase of $R_{\rm AA}$ is visible with decreasing $p_{\rm T}$, which was already observed for the most central events (0–20%) and reported in ref. [17]. Within uncertainties, the results are compatible with those obtained, in a more restricted $p_{\rm T}$ interval, at the lower LHC energy, with a possible hint (1.2σ) of a weaker suppression in the region $2 < p_{\rm T} < 6\,\text{GeV}/c$. The transport model calculations are in qualitative agreement with the data. In this model, a competition between suppression and regeneration of charmonia is assumed, choosing a $\rm c\bar{c}$ production cross section $\rm d\sigma_{c\bar{c}}/d$$y$ = 0.57 mb and $\rm d\sigma^{pp}_{J/\psi}/d$$y$ = 3.35 μb for $2.5 < y < 4$. The latter value is ∼10% smaller than our measurement of the same quantity [17]. The model also includes contributions from both prompt and non-prompt J/ψ. The upper (lower) limit of this calculation corresponds to a 10% (25%) contribution of nuclear shadowing.

Figure 3 shows that, in the explored rapidity interval, there is no significant variation of the $R_{\rm AA}$ values. The calculations of the transport model are in good agreement with the experimental results. The comparison of the results with those obtained at $\sqrt{s_{\rm NN}} = 2.76\,\text{TeV}$ [14] hints (1.5σ) for a weaker suppression at $\sqrt{s_{\rm NN}} = 5.02\,\text{TeV}$ at large y ($3.75 < y < 4$).

4.1.2 Centrality-differential $R_{\rm AA}$ as a function of y and $p_{\rm t}$

Figures 4 and 5 show, respectively, the $p_{\rm T}$ and y dependence of the inclusive J/ψ $R_{\rm AA}$, for events corresponding to the centrality classes 0–20%, 20–40% and 40–90%. It is worth

JHEP02(2020)041

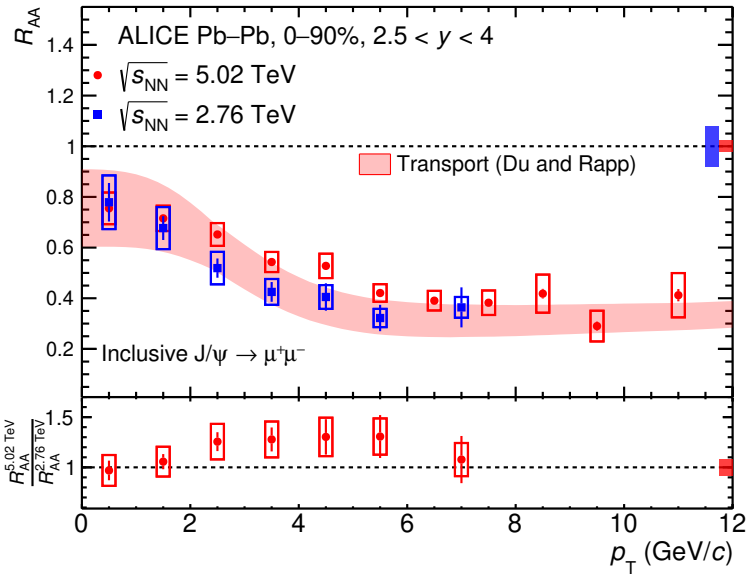


Figure 2. Inclusive J/ψ nuclear modification factor as a function of p_{T} for Pb–Pb collisions at $\sqrt{s_{\mathrm{NN}}} = 5.02\,\mathrm{TeV}$ in the 0–90% centrality class. The vertical error bars represent statistical uncertainties, the boxes around the points uncorrelated systematic uncertainties, while the correlated uncertainty is shown as a filled box around $R_{\mathrm{AA}} = 1$. The corresponding measurements in Pb–Pb collisions at $\sqrt{s_{\mathrm{NN}}} = 2.76\,\mathrm{TeV}$ [14] are also shown, as well as the ratio of the R_{AA} values, which is depicted in the bottom panel of the figure. The R_{AA} values at $\sqrt{s_{\mathrm{NN}}} = 5.02\,\mathrm{TeV}$ are compared with transport model calculations [28].

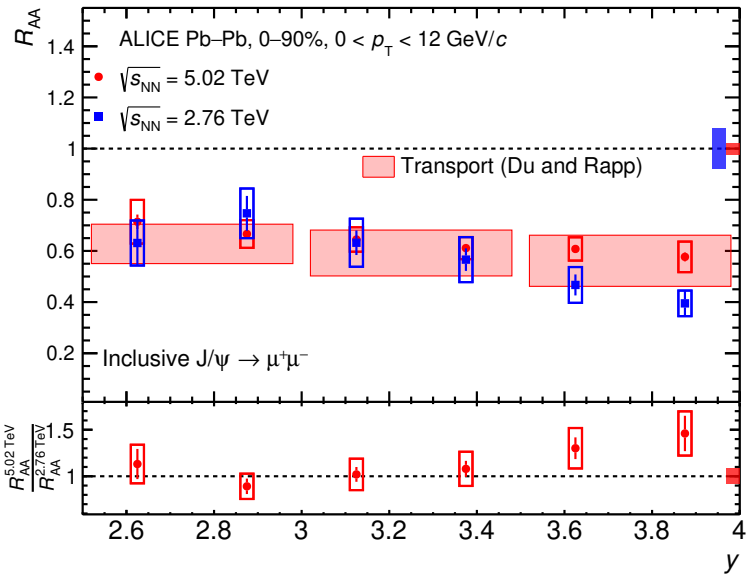


Figure 3. Inclusive J/ψ nuclear modification factor as a function of rapidity for Pb–Pb collisions at $\sqrt{s_{\mathrm{NN}}} = 5.02\,\mathrm{TeV}$ in the 0–90% centrality class. The vertical error bars represent statistical uncertainties, the boxes around the points uncorrelated systematic uncertainties, while the correlated uncertainty is shown as a filled box around $R_{\mathrm{AA}} = 1$. The corresponding measurements in Pb–Pb collisions at $\sqrt{s_{\mathrm{NN}}} = 2.76\,\mathrm{TeV}$ [14] are also shown, as well as the ratio of the R_{AA} values, which is depicted in the bottom panel of the figure. The R_{AA} values at $\sqrt{s_{\mathrm{NN}}} = 5.02\,\mathrm{TeV}$ are compared with transport model calculations [28].

JHEP02(2020)041

noting that the results for 0–20% were already published in ref. [17]. In this paper, the corresponding values were updated with the improved $\langle T_{\rm AA}\rangle$ uncertainties reported in ref. [49]. In Figure 4, moving from central to peripheral collisions, a weaker $p_{\rm T}$ dependence of the $R_{\rm AA}$ is observed, up to an almost constant nuclear modification factor for 40–90% centrality. When comparing results at $\sqrt{s_{\rm NN}} = 5.02\,\text{TeV}$ and 2.76 TeV, a slight increase of the $R_{\rm AA}$ is visible for the most central collisions and for $2 < p_{\rm T} < 6\,\text{GeV}/c$ at the higher collision energy, while the results are compatible in the 20–40% and 40–90% samples. A fair agreement with the transport model calculations is observed. The results for the 0–20% and 20–40% centrality classes are also compared with a model based on statistical hadronization (SHM) [67]. A good agreement with this calculation, which does not include contributions from non-prompt J/ψ production, can be found up to $p_{\rm T} \sim 4\,\text{GeV}/c$, while at higher transverse momentum $R_{\rm AA}$ is underestimated. This feature could partly be due to additional production mechanisms, not implemented in the model, such as J/ψ production from gluon fragmentation in jets.

In figure 5, the $R_{\rm AA}$ values exhibit a very weak rapidity dependence in all the centrality classes, as also observed in 0–90% (figure 3). The calculation of the transport model is able to describe the data, in particular when a weak nuclear shadowing scenario (10%, corresponding to the lower limit chosen by the authors) is adopted.

4.1.3 Centrality dependence of $R_{\rm AA}$

In figures 6 and 7 the $R_{\rm AA}$ as a function of the average number of participant nucleons $\langle N_{\rm part}\rangle$ is shown for various transverse momentum and rapidity intervals, respectively. The $\langle N_{\rm part}\rangle$ intervals correspond to the centrality selections 0–10%, 10–20%, 20–30%, 30–40%, 40–50%, 50–60%, and 60–90%, from larger to smaller $\langle N_{\rm part}\rangle$ values. The results of figure 6 clearly show that moving from low to high $p_{\rm T}$ the centrality dependence of $R_{\rm AA}$ becomes steeper, with $R_{\rm AA}$ reaching a minimum value of $0.29 \pm 0.02(\text{stat}) \pm 0.01(\text{syst})$ for the 0–10% centrality class and $8 < p_{\rm T} < 12\,\text{GeV}/c$. In the low-$p_{\rm T}$ region ($0.3 < p_{\rm T} < 2\,\text{GeV}/c$), the $R_{\rm AA}$ has a weak $\langle N_{\rm part}\rangle$ dependence and is compatible with being constant (~ 0.7) for $\langle N_{\rm part}\rangle > 150$. In the most peripheral centrality class, a deviation from unity can be observed, in particular for $p_{\rm T} > 2\,\text{GeV}/c$, not seen in the theoretical calculations. As discussed in refs. [68, 69], the origin may be from the bias introduced by the event selection and collision geometry, which causes an apparent suppression. When comparing the results with those corresponding to Pb–Pb collisions at $\sqrt{s_{\rm NN}} = 2.76\,\text{TeV}$ [14], systematically higher $R_{\rm AA}$ values are found in the $p_{\rm T}$ interval $2 < p_{\rm T} < 5\,\text{GeV}/c$, even if the maximum observed difference is only at 1.5σ level, for the centrality region 0–10%. In all other $p_{\rm T}$ intervals where the comparison is possible, the results at the two energies are compatible. When comparing the results with the transport model calculations, the agreement is good at low $p_{\rm T}$ ($0.3 < p_{\rm T} < 2\,\text{GeV}/c$), while the data lie close to the upper edge of the calculation at higher $p_{\rm T}$.

In figure 7 the centrality dependence of the nuclear modification factor is shown for 3 rapidity intervals. No variation of the suppression pattern against rapidity is observed. The same weak dependence can also be observed with the transport model calculations.

JHEP02(2020)041

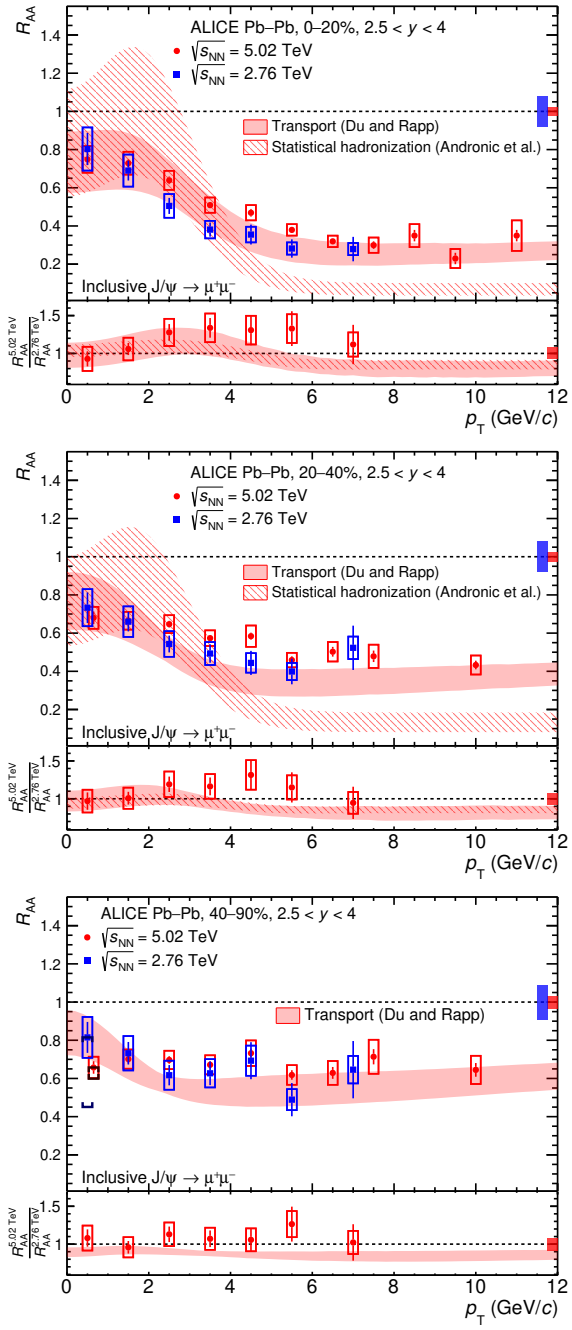


Figure 4. Inclusive J/ψ nuclear modification factor as a function of p_{T} for Pb–Pb collisions at $\sqrt{s_{\mathrm{NN}}} = 5.02\,\mathrm{TeV}$ in the 0–20% (top), 20–40% (middle) and 40–90% (bottom) centrality classes. The vertical error bars represent statistical uncertainties, the boxes around the points uncorrelated systematic uncertainties, while the correlated uncertainty is shown as a filled box around $R_{\mathrm{AA}} = 1$. The corresponding measurements in Pb–Pb collisions at $\sqrt{s_{\mathrm{NN}}} = 2.76\,\mathrm{TeV}$ [14] are also shown, as well as the ratio of the R_{AA} values, which is depicted in the bottom panel of the figure. The R_{AA} values at $\sqrt{s_{\mathrm{NN}}} = 5.02\,\mathrm{TeV}$ and the ratios to lower energy results are compared with transport model calculations [28] and, for 0–20% and 20–40% centrality, with the results of the SHM [67]. The brackets around R_{AA} values for 40–90% centrality in the lowest p_{T} interval represent an estimate of the maximum influence of J/ψ photo-production, as detailed in section 4.1.

JHEP02(2020)041

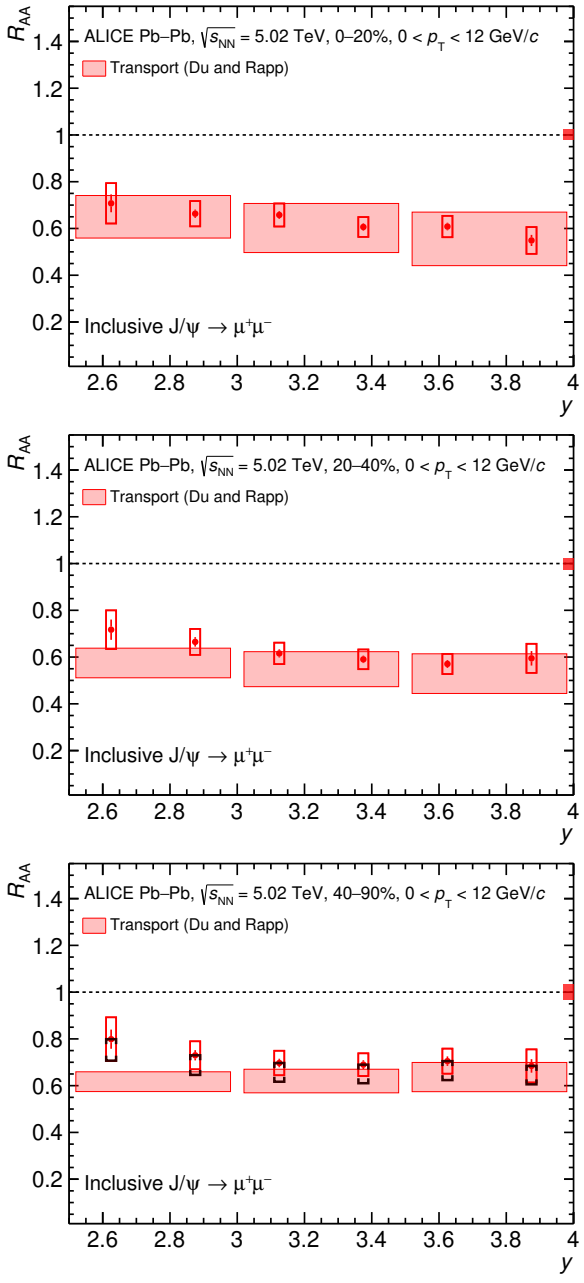


Figure 5. Inclusive J/ψ nuclear modification factor as a function of rapidity for Pb–Pb collisions at $\sqrt{s_{\rm NN}} = 5.02$ TeV in the 0–20% (top), 20–40% (middle) and 40–90% (bottom) centrality classes. The vertical error bars represent statistical uncertainties, the boxes around the points uncorrelated systematic uncertainties, while the correlated uncertainty is shown as a filled box around $R_{\rm AA} = 1$. The $R_{\rm AA}$ values are compared with transport model calculations [28]. The brackets around $R_{\rm AA}$ values for 40–90% centrality represent an estimate of the maximum influence of J/ψ photoproduction, as detailed in section 4.1.

JHEP02(2020)041

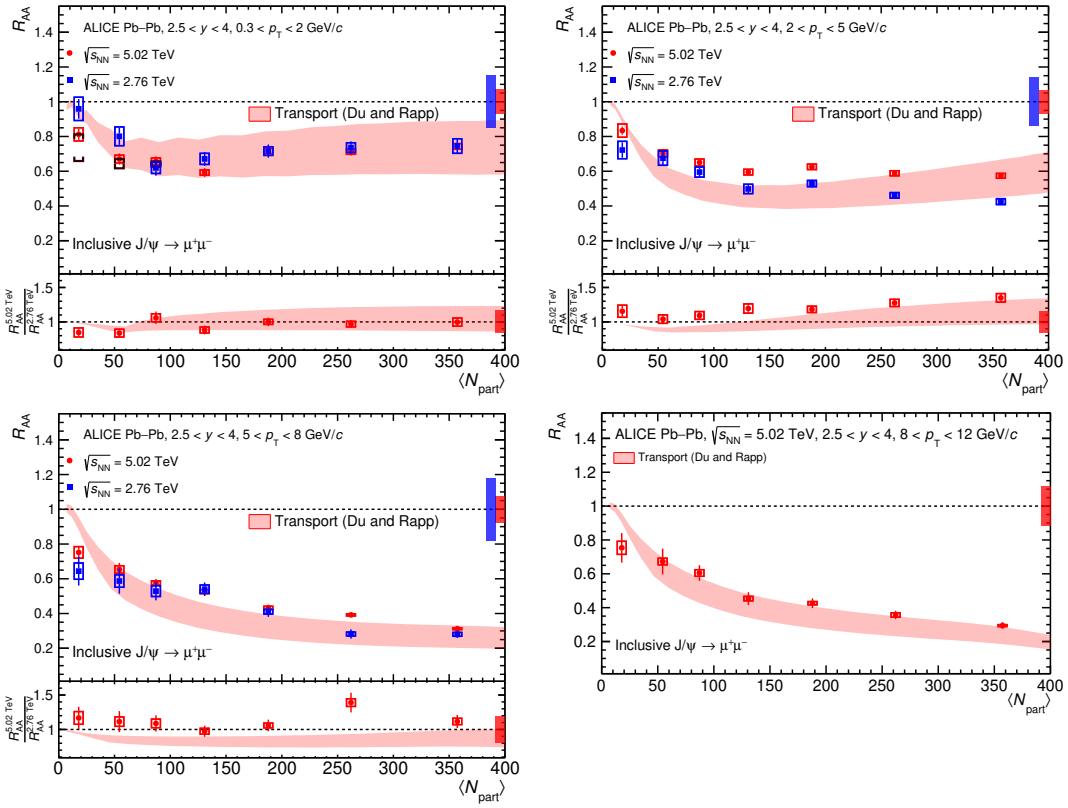


Figure 6. Inclusive J/ψ nuclear modification factor as a function of $\langle N_{\rm part}\rangle$ for Pb–Pb collisions at $\sqrt{s_{\rm NN}} = 5.02\,\text{TeV}$. Results are shown for four $p_{\rm T}$ intervals. The vertical error bars represent statistical uncertainties, the boxes around the points uncorrelated systematic uncertainties, while the correlated uncertainty is shown as a filled box around $R_{\rm AA} = 1$. When the corresponding results at $\sqrt{s_{\rm NN}} = 2.76\,\text{TeV}$ are available, the ratio of the results at the two energies is shown in the bottom section of each figure. The brackets around $R_{\rm AA}$ values for $0.3 < p_{\rm T} < 2\,\text{GeV}/c$ represent an estimate of the influence of J/ψ photo-production, as detailed in section 4.1. The $R_{\rm AA}$ results at $\sqrt{s_{\rm NN}} = 5.02\,\text{TeV}$ as well as the available ratios to the $\sqrt{s_{\rm NN}} = 2.76\,\text{TeV}$ results are compared with transport model calculations [28].

4.2 J/ψ average transverse momentum and $r_{\rm AA}$

A complementary insight into the modification of J/ψ transverse momentum distributions in Pb–Pb collisions can be obtained by the study of the J/ψ average transverse momentum $\langle p_{\rm T}\rangle$ and the average squared momentum $\langle p_{\rm T}^2\rangle$ as a function of the collision centrality. By normalizing $\langle p_{\rm T}^2\rangle$ to the corresponding pp value, one obtains an adimensional quantity, $r_{\rm AA} = \langle {p_{\rm T}}^2\rangle_{\rm AA}/\langle {p_{\rm T}}^2\rangle_{\rm pp}$, useful for comparisons between various collision energies and/or theory calculations.

As a first step, the J/ψ invariant yields as a function of $p_{\rm T}$ are fitted in various centrality classes with the following function

$$f(p_{\rm T}) = C \cdot \frac{p_{\rm T}}{\left(1 + (p_{\rm T}/p_0)^2\right)^n}, \tag{4.2}$$

where C, p_0 and n are free parameters. This function is widely used to reproduce the J/ψ

JHEP02(2020)041

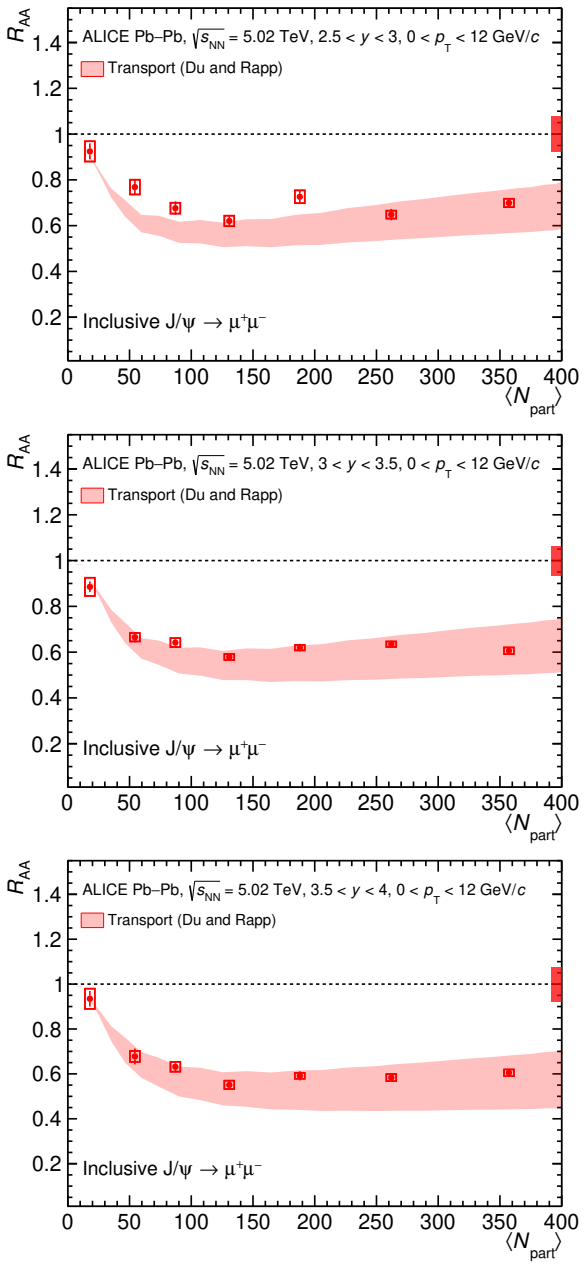


Figure 7. Inclusive J/ψ nuclear modification factor as a function of $\langle N_{\rm part} \rangle$ for Pb–Pb collisions at $\sqrt{s_{\rm NN}} = 5.02\,\text{TeV}$, in the interval $0.3 < p_{\rm T} < 12\,\text{GeV}/c$. Results are shown for three y intervals. The vertical error bars represent statistical uncertainties, the boxes around the points uncorrelated systematic uncertainties, while the correlated uncertainty is shown as a filled box around $R_{\rm AA} = 1$. The results are compared with transport model calculations [28].

JHEP02(2020)041

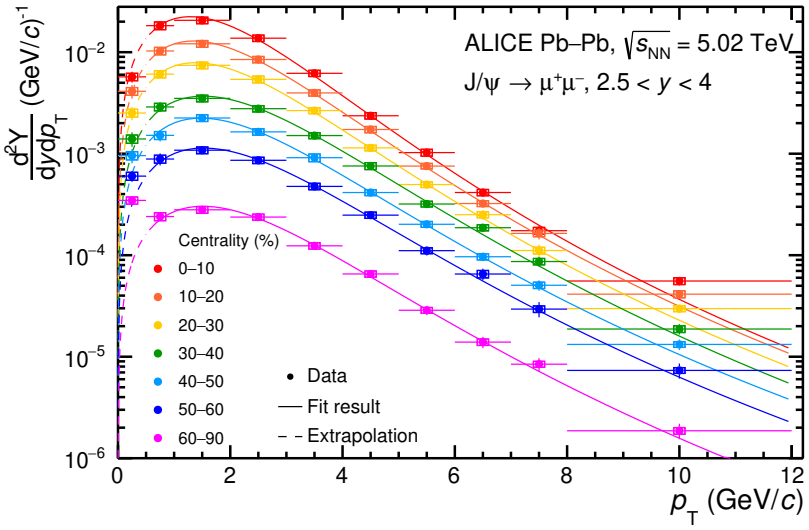


Figure 8. Inclusive J/ψ yields as a function of p_{T} in Pb–Pb collisions at $\sqrt{s_{\mathrm{NN}}} = 5.02\,\mathrm{TeV}$, for various centrality classes. The vertical error bars represent the statistical uncertainties while the uncorrelated systematic uncertainties are represented by boxes around the points. The curves are the results of fits obtained using the function shown in eq. (4.2). The dashed region corresponds to the region $p_{\mathrm{T}} < 0.5\,\mathrm{GeV}/c$, excluded in the fits.

p_{T} distribution in hadronic collisions (e.g refs. [70, 71]). The quantities to be determined, $\langle p_{\mathrm{T}} \rangle$ and $\langle p_{\mathrm{T}}^2 \rangle$, are then computed as the first and second moment of $f(p_{\mathrm{T}})$ respectively. In figure 8, the J/ψ invariant yields as a function of p_{T} are shown for various centrality classes together with the fitted functions. In order to limit the influence of the J/ψ production excess at low p_{T}, due to photo-production, the interval $p_{\mathrm{T}} < 0.5\,\mathrm{GeV}/c$ was excluded from the fit. The statistical (systematic) uncertainties on $\langle p_{\mathrm{T}} \rangle$ and $\langle p_{\mathrm{T}}^2 \rangle$ were obtained from fits to the invariant yield distributions, considering only statistical (p_{T}-uncorrelated systematic) uncertainties on the J/ψ yields.

In the left panel of figure 9, the centrality dependence of $\langle p_{\mathrm{T}} \rangle$ is shown and compared with previous results at $\sqrt{s_{\mathrm{NN}}} = 2.76\,\mathrm{TeV}$ [14]. The centrality dependence of the $\sqrt{s_{\mathrm{NN}}} = 5.02\,\mathrm{TeV}$ results is weak up to $\langle N_{\mathrm{part}} \rangle \sim 150$, followed by a significant decrease towards central events. This softening of the J/ψ p_{T} distributions is a direct consequence of the smaller suppression observed at low p_{T} when considering the transverse-momentum dependence of the nuclear modification factors, shown in figure 4. The $\langle p_{\mathrm{T}} \rangle$ values are systematically larger than those at $\sqrt{s_{\mathrm{NN}}} = 2.76\,\mathrm{TeV}$, an effect due to the increase of the collision energy, but the decrease of $\langle p_{\mathrm{T}} \rangle$ with increasing centrality is similar at the two energies. A more direct comparison with lower energy results and theoretical calculations can be performed by studying the quantity r_{AA}. The results are shown in the right panel of figure 9, and compared with those obtained in Pb–Pb collisions at $\sqrt{s_{\mathrm{NN}}} = 2.76\,\mathrm{TeV}$ and the transport model calculations. In peripheral collisions, and up to $\langle N_{\mathrm{part}} \rangle \sim 150$, the r_{AA} value is compatible with unity within uncertainties. A maximum decrease of ∼25% is observed for central collisions. The brackets around the $\langle p_{\mathrm{T}} \rangle$ and r_{AA} in peripheral collisions represent the possible variation of the hadronic J/ψ $\langle p_{\mathrm{T}} \rangle$ and r_{AA} for two extreme hypothe-

JHEP02(2020)041

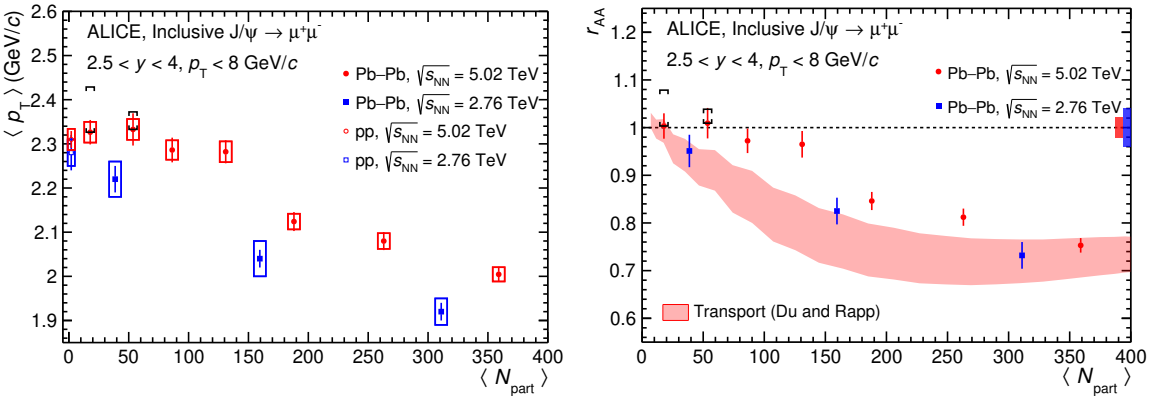


Figure 9. (Left) Inclusive J/ψ $\langle p_{\mathrm{T}} \rangle$ measured in Pb–Pb collisions at $\sqrt{s_{\mathrm{NN}}} = 5.02\,\mathrm{TeV}$ and $\sqrt{s_{\mathrm{NN}}} = 2.76\,\mathrm{TeV}$, as a function of $\langle N_{\mathrm{part}} \rangle$ for $p_{\mathrm{T}} < 8\,\mathrm{GeV}/c$. The vertical error bars represent the statistical uncertainties, while the uncorrelated systematic uncertainties are shown as boxes around the points. J/ψ $\langle p_{\mathrm{T}} \rangle$ results in pp collisions at the two collision energies are also shown at $\langle N_{\mathrm{part}} \rangle = 2$. (Right) Inclusive J/$\psi$ r_{AA} in Pb–Pb collisions at $\sqrt{s_{\mathrm{NN}}} = 5.02\,\mathrm{TeV}$, compared with the $\sqrt{s_{\mathrm{NN}}} = 2.76\,\mathrm{TeV}$ results and a transport model calculation [28], as a function of $\langle N_{\mathrm{part}} \rangle$ for $p_{\mathrm{T}} < 8\,\mathrm{GeV}/c$. The vertical error bars represent the quadratic sum of statistical and systematic uncertainties on the numerator of the r_{AA} expression ($\langle {p_{\mathrm{T}}}^2 \rangle_{\mathrm{AA}}$), while the uncertainties on the denominator ($\langle {p_{\mathrm{T}}}^2 \rangle_{\mathrm{pp}}$) are shown as a filled box around unity. In the two panels, the brackets around the two most peripheral data points represent an estimate of the maximum influence of J/ψ photo-production, as detailed in section 4.2.

ses on the J/ψ photo-production contamination. The lower limit bracket corresponds to the assumption of no contribution from photo-produced J/ψ, while the upper one corresponds to the hypothesis that all the J/ψ with $p_{\mathrm{T}} < 300$ MeV/c are photo-produced. The results are compatible with those at $\sqrt{s_{\mathrm{NN}}} = 2.76\,\mathrm{TeV}$, with a hint for larger r_{AA} values at $\sqrt{s_{\mathrm{NN}}} = 5.02\,\mathrm{TeV}$. A very different centrality dependence was observed at lower collision energies ($\sqrt{s_{\mathrm{NN}}} = 200\,\mathrm{GeV}$ at RHIC [72] and $\sqrt{s_{\mathrm{NN}}} = 17\,\mathrm{GeV}$ at SPS [73]) as the r_{AA} increases (especially at the SPS energy) towards more central collisions (the comparison was shown in ref. [14]). The different behaviors of r_{AA} at different energies can be explained by the increasing amount of J/ψ regeneration with collision energy. Finally, the comparison with the transport model calculation [28] shows good agreement for peripheral and central collisions, but an underestimation of the data points is observed in the intermediate centrality class, reaching a significance up to 2.5σ for $\langle N_{\mathrm{part}} \rangle \sim 150$.

5 Conclusions

This paper reports on ALICE measurements of the inclusive J/ψ production in Pb–Pb collisions at $\sqrt{s_{\mathrm{NN}}} = 5.02\,\mathrm{TeV}$ in the kinematic range $2.5 < y < 4$ up to $p_{\mathrm{T}} < 12\,\mathrm{GeV}/c$. Results on the nuclear modification factor R_{AA}, the average transverse-momentum $\langle p_{\mathrm{T}} \rangle$, and the ratio r_{AA} were presented. A systematic comparison with the calculation of a transport model was carried out and, for the p_{T} dependence of R_{AA}, with the results of a statistical hadronization model.

JHEP02(2020)041

The inclusive J/ψ $R_{\rm AA}$ as a function of transverse momentum and rapidity for the centrality range 0–90%, is compatible with previously published results at $\sqrt{s_{\rm NN}}$ = 2.76 TeV [14]. A suppression of the J/ψ production is observed ($R_{\rm AA}< 1$), mild at low $p_{\rm T}$ but increasing towards higher $p_{\rm T}$, and not strongly depending on rapidity. The centrality-differential studies show that the y dependence of $R_{\rm AA}$ is weak and fairly independent of centrality, while the $p_{\rm T}$ dependence of $R_{\rm AA}$ grows steeper for more central events. All the $R_{\rm AA}$ results are fairly reproduced by the calculation of a transport model, with a tendency to underestimate the observed $R_{\rm AA}$ at intermediate $p_{\rm T}$. The statistical hadronization model reproduces, although with larger uncertainties, the $p_{\rm T}$ dependence of $R_{\rm AA}$ for various centrality classes, but shows a discrepancy in the high-$p_{\rm T}$ region.

A complementary study was also carried out by measuring the centrality dependence of $R_{\rm AA}$ for different $p_{\rm T}$ and y intervals. A suppression strongly increasing with centrality is visible at high $p_{\rm T}$, while at low $p_{\rm T}$ the suppression is relatively weak ($R_{\rm AA} \sim 0.7$) and practically independent of centrality. On the contrary, the shape of the $R_{\rm AA}$ as a function of centrality does not vary significantly in the studied rapidity ranges, showing a mild decrease until $\langle N_{\rm part}\rangle \sim 100$, followed by a plateau.

Finally, the $r_{\rm AA}$ ratio decreases with increasing centrality, similarly to previous observations at $\sqrt{s_{\rm NN}}$ = 2.76 TeV. The transport model calculation underestimates the measurement at intermediate $\langle N_{\rm part}\rangle$ values.

The results shown in this paper confirm, with better accuracy, the observations carried out at $\sqrt{s_{\rm NN}}$ = 2.76 TeV and strengthen the evidence for the presence of a mechanism that leads to a significant increase of $R_{\rm AA}$ at low $p_{\rm T}$. Recombination of charm-quark pairs during the deconfined QGP phase, as implemented in the transport model compared with our results, is a strong candidate for explaining the features of the data.

Acknowledgments

The ALICE Collaboration would like to thank all its engineers and technicians for their invaluable contributions to the construction of the experiment and the CERN accelerator teams for the outstanding performance of the LHC complex. The ALICE Collaboration gratefully acknowledges the resources and support provided by all Grid centres and the Worldwide LHC Computing Grid (WLCG) collaboration. The ALICE Collaboration acknowledges the following funding agencies for their support in building and running the ALICE detector: A. I. Alikhanyan National Science Laboratory (Yerevan Physics Institute) Foundation (ANSL), State Committee of Science and World Federation of Scientists (WFS), Armenia; Austrian Academy of Sciences, Austrian Science Fund (FWF): [M 2467-N36] and Nationalstiftung für Forschung, Technologie und Entwicklung, Austria; Ministry of Communications and High Technologies, National Nuclear Research Center, Azerbaijan; Conselho Nacional de Desenvolvimento Científico e Tecnológico (CNPq), Financiadora de Estudos e Projetos (Finep), Fundação de Amparo à Pesquisa do Estado de São Paulo (FAPESP) and Universidade Federal do Rio Grande do Sul (UFRGS), Brazil; Ministry of Education of China (MOEC), Ministry of Science & Technology of China (MSTC) and National Natural Science Foundation of China (NSFC), China; Ministry of Science

JHEP02(2020)041

and Education and Croatian Science Foundation, Croatia; Centro de Aplicaciones Tecnológicas y Desarrollo Nuclear (CEADEN), Cubaenergía, Cuba; Ministry of Education, Youth and Sports of the Czech Republic, Czech Republic; The Danish Council for Independent Research — Natural Sciences, the VILLUM FONDEN and Danish National Research Foundation (DNRF), Denmark; Helsinki Institute of Physics (HIP), Finland; Commissariat à l'Energie Atomique (CEA), Institut National de Physique Nucléaire et de Physique des Particules (IN2P3) and Centre National de la Recherche Scientifique (CNRS) and Région des Pays de la Loire, France; Bundesministerium für Bildung und Forschung (BMBF) and GSI Helmholtzzentrum für Schwerionenforschung GmbH, Germany; General Secretariat for Research and Technology, Ministry of Education, Research and Religions, Greece; National Research, Development and Innovation Office, Hungary; Department of Atomic Energy Government of India (DAE), Department of Science and Technology, Government of India (DST), University Grants Commission, Government of India (UGC) and Council of Scientific and Industrial Research (CSIR), India; Indonesian Institute of Science, Indonesia; Centro Fermi — Museo Storico della Fisica e Centro Studi e Ricerche Enrico Fermi and Istituto Nazionale di Fisica Nucleare (INFN), Italy; Institute for Innovative Science and Technology, Nagasaki Institute of Applied Science (IIST), Japanese Ministry of Education, Culture, Sports, Science and Technology (MEXT) and Japan Society for the Promotion of Science (JSPS) KAKENHI, Japan; Consejo Nacional de Ciencia (CONACYT) y Tecnología, through Fondo de Cooperación Internacional en Ciencia y Tecnología (FONCICYT) and Dirección General de Asuntos del Personal Academico (DGAPA), Mexico; Nederlandse Organisatie voor Wetenschappelijk Onderzoek (NWO), Netherlands; The Research Council of Norway, Norway; Commission on Science and Technology for Sustainable Development in the South (COMSATS), Pakistan; Pontificia Universidad Católica del Perú, Peru; Ministry of Science and Higher Education and National Science Centre, Poland; Korea Institute of Science and Technology Information and National Research Foundation of Korea (NRF), Republic of Korea; Ministry of Education and Scientific Research, Institute of Atomic Physics and Ministry of Research and Innovation and Institute of Atomic Physics, Romania; Joint Institute for Nuclear Research (JINR), Ministry of Education and Science of the Russian Federation, National Research Centre Kurchatov Institute, Russian Science Foundation and Russian Foundation for Basic Research, Russia; Ministry of Education, Science, Research and Sport of the Slovak Republic, Slovakia; National Research Foundation of South Africa, South Africa; Swedish Research Council (VR) and Knut & Alice Wallenberg Foundation (KAW), Sweden; European Organization for Nuclear Research, Switzerland; Suranaree University of Technology (SUT), National Science and Technology Development Agency (NSDTA) and Office of the Higher Education Commission under NRU project of Thailand, Thailand; Turkish Atomic Energy Agency (TAEK), Turkey; National Academy of Sciences of Ukraine, Ukraine; Science and Technology Facilities Council (STFC), United Kingdom; National Science Foundation of the United States of America (NSF) and United States Department of Energy, Office of Nuclear Physics (DOE NP), United States of America.

JHEP02(2020)041

Open Access. This article is distributed under the terms of the Creative Commons Attribution License (CC-BY 4.0), which permits any use, distribution and reproduction in any medium, provided the original author(s) and source are credited.

References

[1] HotQCD collaboration, *Equation of state in* $(2+1)$*-flavor QCD*, *Phys. Rev.* **D 90** (2014) 094503 [arXiv:1407.6387] [INSPIRE].

[2] S. Borsányi, Z. Fodor, C. Hölbling, S.D. Katz, S. Krieg and K.K. Szabo, *Full result for the QCD equation of state with 2+1 flavors*, *Phys. Lett.* **B 730** (2014) 99 [arXiv:1309.5258] [INSPIRE].

[3] P. Braun-Munzinger, V. Koch, T. Schäfer and J. Stachel, *Properties of hot and dense matter from relativistic heavy ion collisions*, *Phys. Rept.* **621** (2016) 76 [arXiv:1510.00442] [INSPIRE].

[4] T. Matsui and H. Satz, *J/ψ Suppression by Quark-Gluon Plasma Formation*, *Phys. Lett.* **B 178** (1986) 416 [INSPIRE].

[5] S. Digal, P. Petreczky and H. Satz, *Quarkonium feed down and sequential suppression*, *Phys. Rev.* **D 64** (2001) 094015 [hep-ph/0106017] [INSPIRE].

[6] NA50 collaboration, *A new measurement of J/ψ suppression in Pb-Pb collisions at 158 GeV per nucleon*, *Eur. Phys. J.* **C 39** (2005) 335 [hep-ex/0412036] [INSPIRE].

[7] NA60 collaboration, *J/ψ production in indium-indium collisions at 158 GeV/nucleon*, *Phys. Rev. Lett.* **99** (2007) 132302 [INSPIRE].

[8] PHENIX collaboration, *J/ψ Production vs Centrality, Transverse Momentum, and Rapidity in Au+Au Collisions at* $\sqrt{s_{NN}} = 200$ *GeV*, *Phys. Rev. Lett.* **98** (2007) 232301 [nucl-ex/0611020] [INSPIRE].

[9] PHENIX collaboration, *J/ψ suppression at forward rapidity in Au+Au collisions at* $\sqrt{s_{NN}} = 200$ *GeV*, *Phys. Rev.* **C 84** (2011) 054912 [arXiv:1103.6269] [INSPIRE].

[10] STAR collaboration, *Energy dependence of J/ψ production in Au+Au collisions at* $\sqrt{s_{NN}} = 39$*,* 62.4 *and* 200 *GeV*, *Phys. Lett.* **B 771** (2017) 13 [arXiv:1607.07517] [INSPIRE].

[11] STAR collaboration, *J/ψ production at high transverse momentum in p+p and Cu+Cu collisions at* $\sqrt{s_{\rm NN}} = 200$ *GeV*, *Phys. Rev.* **C 80** (2009) 041902 [arXiv:0904.0439] [INSPIRE].

[12] ALICE collaboration, *Centrality, rapidity and transverse momentum dependence of J/ψ suppression in Pb-Pb collisions at* $\sqrt{s_{\rm NN}} = 2.76$ *TeV*, *Phys. Lett.* **B 734** (2014) 314 [arXiv:1311.0214] [INSPIRE].

[13] ALICE collaboration, *J/ψ Suppression at Forward Rapidity in Pb-Pb Collisions at* $\sqrt{s_{\rm NN}} = 2.76$ *TeV*, *Phys. Rev. Lett.* **109** (2012) 072301 [arXiv:1202.1383] [INSPIRE].

[14] ALICE collaboration, *Differential studies of inclusive J/ψ and ψ(2S) production at forward rapidity in Pb-Pb collisions at* $\sqrt{s_{\rm NN}} = 2.76$ *TeV*, *JHEP* **05** (2016) 179 [arXiv:1506.08804] [INSPIRE].

[15] ALICE collaboration, *Inclusive, prompt and non-prompt J/ψ production at mid-rapidity in Pb-Pb collisions at* $\sqrt{s_{\rm NN}} = 2.76$ *TeV*, *JHEP* **07** (2015) 051 [arXiv:1504.07151] [INSPIRE].

[16] CMS collaboration, *Suppression of non-prompt J/ψ, prompt J/ψ, and Y(1S) in PbPb collisions at* $\sqrt{s_{NN}} = 2.76$ *TeV*, *JHEP* **05** (2012) 063 [arXiv:1201.5069] [INSPIRE].

[17] ALICE collaboration, *J/ψ suppression at forward rapidity in Pb-Pb collisions at* $\sqrt{s_{\rm NN}} = 5.02$ *TeV*, *Phys. Lett.* **B 766** (2017) 212 [arXiv:1606.08197] [INSPIRE].

JHEP02(2020)041

[18] CMS collaboration, *Measurement of prompt and nonprompt charmonium suppression in PbPb collisions at 5.02 TeV*, *Eur. Phys. J.* **C 78** (2018) 509 [arXiv:1712.08959] [INSPIRE].

[19] ATLAS collaboration, *Prompt and non-prompt J/ψ and ψ(2S) suppression at high transverse momentum in* 5.02 TeV *Pb+Pb collisions with the ATLAS experiment*, *Eur. Phys. J.* **C 78** (2018) 762 [arXiv:1805.04077] [INSPIRE].

[20] M.L. Miller, K. Reygers, S.J. Sanders and P. Steinberg, *Glauber modeling in high energy nuclear collisions*, *Ann. Rev. Nucl. Part. Sci.* **57** (2007) 205 [nucl-ex/0701025] [INSPIRE].

[21] R.L. Thews, M. Schroedter and J. Rafelski, *Enhanced J/ψ production in deconfined quark matter*, *Phys. Rev.* **C 63** (2001) 054905 [hep-ph/0007323] [INSPIRE].

[22] P. Braun-Munzinger and J. Stachel, *(Non)thermal aspects of charmonium production and a new look at J/ψ suppression*, *Phys. Lett.* **B 490** (2000) 196 [nucl-th/0007059] [INSPIRE].

[23] ALICE collaboration, *J/ψ Elliptic Flow in Pb-Pb Collisions at $\sqrt{s_{\rm NN}} = 2.76$ TeV*, *Phys. Rev. Lett.* **111** (2013) 162301 [arXiv:1303.5880] [INSPIRE].

[24] CMS collaboration, *Suppression and azimuthal anisotropy of prompt and nonprompt* J/ψ *production in PbPb collisions at $\sqrt{s_{_{NN}}} = 2.76$ TeV*, *Eur. Phys. J.* **C 77** (2017) 252 [arXiv:1610.00613] [INSPIRE].

[25] ALICE collaboration, *J/ψ elliptic flow in Pb-Pb collisions at $\sqrt{s_{\rm NN}} = 5.02$ TeV*, *Phys. Rev. Lett.* **119** (2017) 242301 [arXiv:1709.05260] [INSPIRE].

[26] ALICE collaboration, *Study of J/ψ azimuthal anisotropy at forward rapidity in Pb-Pb collisions at $\sqrt{s_{\rm NN}} = 5.02$ TeV*, *JHEP* **02** (2019) 012 [arXiv:1811.12727] [INSPIRE].

[27] ATLAS collaboration, *Prompt and non-prompt J/ψ elliptic flow in Pb+Pb collisions at $\sqrt{s_{_{NN}}} = 5.02$ TeV with the ATLAS detector*, *Eur. Phys. J.* **C 78** (2018) 784 [arXiv:1807.05198] [INSPIRE].

[28] X. Du and R. Rapp, *Sequential Regeneration of Charmonia in Heavy-Ion Collisions*, *Nucl. Phys.* **A 943** (2015) 147 [arXiv:1504.00670] [INSPIRE].

[29] Y.-p. Liu, Z. Qu, N. Xu and P.-f. Zhuang, *J/ψ Transverse Momentum Distribution in High Energy Nuclear Collisions at RHIC*, *Phys. Lett.* **B 678** (2009) 72 [arXiv:0901.2757] [INSPIRE].

[30] K.J. Eskola, P. Paakkinen, H. Paukkunen and C.A. Salgado, *EPPS16: Nuclear parton distributions with LHC data*, *Eur. Phys. J.* **C 77** (2017) 163 [arXiv:1612.05741] [INSPIRE].

[31] K. Kovarik et al., *nCTEQ15 — Global analysis of nuclear parton distributions with uncertainties in the CTEQ framework*, *Phys. Rev.* **D 93** (2016) 085037 [arXiv:1509.00792] [INSPIRE].

[32] ALICE collaboration, *J/ψ production and nuclear effects in p-Pb collisions at $\sqrt{S_{NN}} = 5.02$ TeV*, *JHEP* **02** (2014) 073 [arXiv:1308.6726] [INSPIRE].

[33] ALICE collaboration, *Inclusive J/ψ production at forward and backward rapidity in p-Pb collisions at $\sqrt{s_{\rm NN}} = 8.16$ TeV*, *JHEP* **07** (2018) 160 [arXiv:1805.04381] [INSPIRE].

[34] CMS collaboration, *Measurement of prompt and nonprompt* J/ψ *production in* pp *and* pPb *collisions at $\sqrt{s_{\rm NN}} = 5.02$ TeV*, *Eur. Phys. J.* **C 77** (2017) 269 [arXiv:1702.01462] [INSPIRE].

[35] ALICE collaboration, *Rapidity and transverse-momentum dependence of the inclusive J/ψ nuclear modification factor in p-Pb collisions at $\sqrt{s_{N\ N}} = 5.02$ TeV*, *JHEP* **06** (2015) 055 [arXiv:1503.07179] [INSPIRE].

JHEP02(2020)041

[36] LHCb collaboration, *Prompt and nonprompt J/ψ production and nuclear modification in pPb collisions at $\sqrt{s_{NN}} = 8.16$ TeV*, *Phys. Lett.* **B 774** (2017) 159 [arXiv:1706.07122] [INSPIRE].

[37] ATLAS collaboration, *Measurement of quarkonium production in proton-lead and proton-proton collisions at 5.02 TeV with the ATLAS detector*, *Eur. Phys. J.* **C 78** (2018) 171 [arXiv:1709.03089] [INSPIRE].

[38] A. Andronic et al., *Heavy-flavour and quarkonium production in the LHC era: from proton-proton to heavy-ion collisions*, *Eur. Phys. J.* **C 76** (2016) 107 [arXiv:1506.03981] [INSPIRE].

[39] ALICE collaboration, *The ALICE experiment at the CERN LHC*, 2008 *JINST* **3** S08002 [INSPIRE].

[40] ALICE collaboration, *Performance of the ALICE Experiment at the CERN LHC*, *Int. J. Mod. Phys.* **A 29** (2014) 1430044 [arXiv:1402.4476] [INSPIRE].

[41] ALICE collaboration, *Alignment of the ALICE Inner Tracking System with cosmic-ray tracks*, 2010 *JINST* **5** P03003 [arXiv:1001.0502] [INSPIRE].

[42] ALICE collaboration, *Performance of the ALICE VZERO system*, 2013 *JINST* **8** P10016 [arXiv:1306.3130] [INSPIRE].

[43] M. Bondila et al., *ALICE T0 detector*, *IEEE Trans. Nucl. Sci.* **52** (2005) 1705.

[44] ALICE collaboration, *Measurement of the Cross Section for Electromagnetic Dissociation with Neutron Emission in Pb-Pb Collisions at $\sqrt{s_{NN}} = 2.76$ TeV*, *Phys. Rev. Lett.* **109** (2012) 252302 [arXiv:1203.2436] [INSPIRE].

[45] ALICE collaboration, *Centrality determination of Pb-Pb collisions at $\sqrt{s_{\rm NN}} = 2.76$ TeV with ALICE*, *Phys. Rev.* **C 88** (2013) 044909 [arXiv:1301.4361] [INSPIRE].

[46] ALICE collaboration, *Centrality dependence of the charged particle multiplicity density at midrapidity in Pb-Pb collisions at $\sqrt{s_{\rm NN}} = 5.02$ TeV*, *Phys. Rev. Lett.* **116** (2016) 222302 [arXiv:1512.06104] [INSPIRE].

[47] ALICE collaboration, *Performance of the RPC-based ALICE muon trigger system at the LHC*, 2012 *JINST* **7** T12002 [arXiv:1211.1948] [INSPIRE].

[48] Particle Data Group collaboration, *Review of Particle Physics*, *Phys. Rev.* **D 98** (2018) 030001 [INSPIRE].

[49] ALICE collaboration, *Centrality determination in heavy ion collisions*, ALICE-PUBLIC-2018-011.

[50] C. Loizides, J. Kamin and D. d'Enterria, *Improved Monte Carlo Glauber predictions at present and future nuclear colliders*, *Phys. Rev.* **C 97** (2018) 054910 [arXiv:1710.07098] [INSPIRE].

[51] ALICE collaboration, *Energy dependence of forward-rapidity J/ψ and $\psi(2\mathrm{S})$ production in pp collisions at the LHC*, *Eur. Phys. J.* **C 77** (2017) 392 [arXiv:1702.00557] [INSPIRE].

[52] ALICE collaboration, *ALICE luminosity determination for pp collisions at $\sqrt{s} = 5$ TeV*, ALICE-PUBLIC-2016-005.

[53] ALICE collaboration, *Rapidity and transverse momentum dependence of inclusive J/ψ production in pp collisions at $\sqrt{s} = 7$ TeV*, *Phys. Lett.* **B 704** (2011) 442 [*Erratum ibid.* **B 718** (2012) 692] [arXiv:1105.0380] [INSPIRE].

[54] ALICE collaboration, *Quarkonium signal extraction in ALICE*, ALICE-PUBLIC-2015-006.

JHEP02(2020)041

[55] R. Brun, F. Carminati and G. Simone, *GEANT Detector Description and Simulation Tool*, CERN-W-5013.

[56] GEANT4 collaboration, *GEANT4 — A simulation toolkit*, *Nucl. Instrum. Meth.* **A 506** (2003) 250 [INSPIRE].

[57] ALICE collaboration, *Suppression of ψ(2S) production in p-Pb collisions at $\sqrt{s_{\rm NN}} = 5.02$ TeV*, *JHEP* **12** (2014) 073 [arXiv:1405.3796] [INSPIRE].

[58] ALICE collaboration, *J/ψ polarization in pp collisions at $\sqrt{s} = 7$ TeV*, *Phys. Rev. Lett.* **108** (2012) 082001 [arXiv:1111.1630] [INSPIRE].

[59] ALICE collaboration, *Measurement of the inclusive J/ψ polarization at forward rapidity in pp collisions at $\sqrt{\mathbf{s}} = \mathbf{8}$ TeV*, *Eur. Phys. J.* **C 78** (2018) 562 [arXiv:1805.04374] [INSPIRE].

[60] ALICE collaboration, *Measurement of quarkonium production at forward rapidity in pp collisions at $\sqrt{s} = 7$ TeV*, *Eur. Phys. J.* **C 74** (2014) 2974 [arXiv:1403.3648] [INSPIRE].

[61] LHCb collaboration, *Measurement of J/ψ production in pp collisions at $\sqrt{s} = 7$ TeV*, *Eur. Phys. J.* **C 71** (2011) 1645 [arXiv:1103.0423] [INSPIRE].

[62] LHCb collaboration, *Measurement of J/ψ production in pp collisions at $\sqrt{s} = 2.76$ TeV*, *JHEP* **02** (2013) 041 [arXiv:1212.1045] [INSPIRE].

[63] ALICE and LHCb collaborations, *Reference pp cross-sections for J/ψ studies in proton-lead collisions at $\sqrt{s_{NN}} = 5.02$ TeV and comparisons between ALICE and LHCb results*, LHCb-CONF-2013-013 (2013).

[64] ALICE collaboration, *Measurement of an excess in the yield of J/ψ at very low $p_{\rm T}$ in Pb-Pb collisions at $\sqrt{s_{\rm NN}} = 2.76$ TeV*, *Phys. Rev. Lett.* **116** (2016) 222301 [arXiv:1509.08802] [INSPIRE].

[65] ALICE collaboration, *Coherent J/ψ photoproduction in ultra-peripheral Pb-Pb collisions at $\sqrt{s_{NN}} = 2.76$ TeV*, *Phys. Lett.* **B 718** (2013) 1273 [arXiv:1209.3715] [INSPIRE].

[66] X. Zhao and R. Rapp, *Medium Modifications and Production of Charmonia at LHC*, *Nucl. Phys.* **A 859** (2011) 114 [arXiv:1102.2194] [INSPIRE].

[67] A. Andronic, P. Braun-Munzinger, M.K. Köhler, K. Redlich and J. Stachel, *Transverse momentum distributions of charmonium states with the statistical hadronization model*, *Phys. Lett.* **B 797** (2019) 134836 [arXiv:1901.09200] [INSPIRE].

[68] C. Loizides and A. Morsch, *Absence of jet quenching in peripheral nucleus-nucleus collisions*, *Phys. Lett.* **B 773** (2017) 408 [arXiv:1705.08856] [INSPIRE].

[69] ALICE collaboration, *Analysis of the apparent nuclear modification in peripheral Pb-Pb collisions at 5.02 TeV*, *Phys. Lett.* **B 793** (2019) 420 [arXiv:1805.05212] [INSPIRE].

[70] J.K. Yoh et al., *Study of scaling in hadronic production of dimuons*, *Phys. Rev. Lett.* **41** (1978) 684 [*Erratum ibid.* **41** (1978) 1083] [INSPIRE].

[71] F. Bossu, Z.C. del Valle, A. de Falco, M. Gagliardi, S. Grigoryan and G. Martinez Garcia, *Phenomenological interpolation of the inclusive J/ψ cross section to proton-proton collisions at 2.76 TeV and 5.5 TeV*, arXiv:1103.2394 [INSPIRE].

[72] PHENIX collaboration, *J/ψ Production in $\sqrt{s_{NN}} = 200$ GeV Cu + Cu Collisions*, *Phys. Rev. Lett.* **101** (2008) 122301 [arXiv:0801.0220] [INSPIRE].

[73] NA50 collaboration, *Transverse momentum distributions of J/ψ, $\psi(2s)$, Drell-Yan and continuum dimuons produced in Pb-Pb interactions at the SPS*, *Phys. Lett.* **B 499** (2001) 85 [INSPIRE].

JHEP02(2020)041

The ALICE collaboration

S. Acharya[141], D. Adamová[93], S.P. Adhya[141], A. Adler[73], J. Adolfsson[79], M.M. Aggarwal[98], G. Aglieri Rinella[34], M. Agnello[31], N. Agrawal[10,48,53], Z. Ahammed[141], S. Ahmad[17], S.U. Ahn[75], A. Akindinov[90], M. Al-Turany[105], S.N. Alam[141], D.S.D. Albuquerque[122], D. Aleksandrov[86], B. Alessandro[58], H.M. Alfanda[6], R. Alfaro Molina[71], B. Ali[17], Y. Ali[15], A. Alici[10,27,53], A. Alkin[2], J. Alme[22], T. Alt[68], L. Altenkamper[22], I. Altsybeev[112], M.N. Anaam[6], C. Andrei[47], D. Andreou[34], H.A. Andrews[109], A. Andronic[144], M. Angeletti[34], V. Anguelov[102], C. Anson[16], T. Antičić[106], F. Antinori[56], P. Antonioli[53], R. Anwar[125], N. Apadula[78], L. Aphecetche[114], H. Appelshäuser[68], S. Arcelli[27], R. Arnaldi[58], M. Arratia[78], I.C. Arsene[21], M. Arslandok[102], A. Augustinus[34], R. Averbeck[105], S. Aziz[61], M.D. Azmi[17], A. Badalà[55], Y.W. Baek[40], S. Bagnasco[58], X. Bai[105], R. Bailhache[68], R. Bala[99], A. Baldisseri[137], M. Ball[42], S. Balouza[103], R.C. Baral[84], R. Barbera[28], L. Barioglio[26], G.G. Barnaföldi[145], L.S. Barnby[92], V. Barret[134], P. Bartalini[6], K. Barth[34], E. Bartsch[68], F. Baruffaldi[29], N. Bastid[134], S. Basu[143], G. Batigne[114], B. Batyunya[74], P.C. Batzing[21], D. Bauri[48], J.L. Bazo Alba[110], I.G. Bearden[87], C. Bedda[63], N.K. Behera[60], I. Belikov[136], F. Bellini[34], R. Bellwied[125], V. Belyaev[91], G. Bencedi[145], S. Beole[26], A. Bercuci[47], Y. Berdnikov[96], D. Berenyi[145], R.A. Bertens[130], D. Berzano[58], M.G. Besoiu[67], L. Betev[34], A. Bhasin[99], I.R. Bhat[99], M.A. Bhat[3], H. Bhatt[48], B. Bhattacharjee[41], A. Bianchi[26], L. Bianchi[26], N. Bianchi[51], J. Bielčík[37], J. Bielčíková[93], A. Bilandzic[103,117], G. Biro[145], R. Biswas[3], S. Biswas[3], J.T. Blair[119], D. Blau[86], C. Blume[68], G. Boca[139], F. Bock[34,94], A. Bogdanov[91], L. Boldizsár[145], A. Bolozdynya[91], M. Bombara[38], G. Bonomi[140], H. Borel[137], A. Borissov[91,144], M. Borri[127], H. Bossi[146], E. Botta[26], L. Bratrud[68], P. Braun-Munzinger[105], M. Bregant[121], T.A. Broker[68], M. Broz[37], E.J. Brucken[43], E. Bruna[58], G.E. Bruno[33,104], M.D. Buckland[127], D. Budnikov[107], H. Buesching[68], S. Bufalino[31], O. Bugnon[114], P. Buhler[113], P. Buncic[34], Z. Buthelezi[72], J.B. Butt[15], J.T. Buxton[95], S.A. Bysiak[118], D. Caffarri[88], A. Caliva[105], E. Calvo Villar[110], R.S. Camacho[44], P. Camerini[25], A.A. Capon[113], F. Carnesecchi[10,27], J. Castillo Castellanos[137], A.J. Castro[130], E.A.R. Casula[54], F. Catalano[31], C. Ceballos Sanchez[52], P. Chakraborty[48], S. Chandra[141], B. Chang[126], W. Chang[6], S. Chapeland[34], M. Chartier[127], S. Chattopadhyay[141], S. Chattopadhyay[108], A. Chauvin[24], C. Cheshkov[135], B. Cheynis[135], V. Chibante Barroso[34], D.D. Chinellato[122], S. Cho[60], P. Chochula[34], T. Chowdhury[134], P. Christakoglou[88], C.H. Christensen[87], P. Christiansen[79], T. Chujo[133], C. Cicalo[54], L. Cifarelli[10,27], F. Cindolo[53], J. Cleymans[124], F. Colamaria[52], D. Colella[52], A. Collu[78], M. Colocci[27], M. Concas[58, ii], G. Conesa Balbastre[77], Z. Conesa del Valle[61], G. Contin[59,127], J.G. Contreras[37], T.M. Cormier[94], Y. Corrales Morales[26,58], P. Cortese[32], M.R. Cosentino[123], F. Costa[34], S. Costanza[139], P. Crochet[134], E. Cuautle[69], P. Cui[6], L. Cunqueiro[94], D. Dabrowski[142], T. Dahms[103,117], A. Dainese[56], F.P.A. Damas[114,137], S. Dani[65], M.C. Danisch[102], A. Danu[67], D. Das[108], I. Das[108], P. Das[3], S. Das[3], A. Dash[84], S. Dash[48], A. Dashi[103], S. De[49,84], A. De Caro[30], G. de Cataldo[52], C. de Conti[121], J. de Cuveland[39], A. De Falco[24], D. De Gruttola[10], N. De Marco[58], S. De Pasquale[30], R.D. De Souza[122], S. Deb[49], H.F. Degenhardt[121], K.R. Deja[142], A. Deloff[83], S. Delsanto[26,131], D. Devetak[105], P. Dhankher[48], D. Di Bari[33], A. Di Mauro[34], R.A. Diaz[8], T. Dietel[124], P. Dillenseger[68], Y. Ding[6], R. Divià[34], Ø. Djuvsland[22], U. Dmitrieva[62], A. Dobrin[34,67], B. Dönigus[68], B. Audurier[114], O. Dordic[21], A.K. Dubey[141], A. Dubla[105], S. Dudi[98], M. Dukhishyam[84], P. Dupieux[134], R.J. Ehlers[146], D. Elia[52], H. Engel[73], E. Epple[146], B. Erazmus[114], F. Erhardt[97], A. Erokhin[112], M.R. Ersdal[22], B. Espagnon[61], G. Eulisse[34], J. Eum[18], D. Evans[109], S. Evdokimov[89], L. Fabbietti[103,117], M. Faggin[29], J. Faivre[77], F. Fan[6], A. Fantoni[51], M. Fasel[94], P. Fecchio[31], A. Feliciello[58], G. Feofilov[112], A. Fernández Téllez[44], A. Ferrero[137], A. Ferretti[26], A. Festanti[34], V.J.G. Feuillard[102], J. Figiel[118], S. Filchagin[107], D. Finogeev[62], F.M. Fionda[22], G. Fiorenza[52],

JHEP02(2020)041

F. Flor[125], S. Foertsch[72], P. Foka[105], S. Fokin[86], E. Fragiacomo[59], U. Frankenfeld[105], G.G. Fronze[26], U. Fuchs[34], C. Furget[77], A. Furs[62], M. Fusco Girard[30], J.J. Gaardhøje[87], M. Gagliardi[26], A.M. Gago[110], A. Gal[136], C.D. Galvan[120], P. Ganoti[82], C. Garabatos[105], E. Garcia-Solis[11], K. Garg[28], C. Gargiulo[34], A. Garibli[85], K. Garner[144], P. Gasik[103,117], E.F. Gauger[119], M.B. Gay Ducati[70], M. Germain[114], J. Ghosh[108], P. Ghosh[141], S.K. Ghosh[3], P. Gianotti[51], P. Giubellino[58,105], P. Giubilato[29], P. Glässel[102], D.M. Goméz Coral[71], A. Gomez Ramirez[73], V. Gonzalez[105], P. González-Zamora[44], S. Gorbunov[39], L. Görlich[118], S. Gotovac[35], V. Grabski[71], L.K. Graczykowski[142], K.L. Graham[109], L. Greiner[78], A. Grelli[63], C. Grigoras[34], V. Grigoriev[91], A. Grigoryan[1], S. Grigoryan[74], O.S. Groettvik[22], F. Grosa[31], J.F. Grosse-Oetringhaus[34], R. Grosso[105], R. Guernane[77], B. Guerzoni[27], M. Guittiere[114], K. Gulbrandsen[87], T. Gunji[132], A. Gupta[99], R. Gupta[99], I.B. Guzman[44], R. Haake[146], M.K. Habib[105], C. Hadjidakis[61], H. Hamagaki[80], G. Hamar[145], M. Hamid[6], R. Hannigan[119], M.R. Haque[63], A. Harlenderova[105], J.W. Harris[146], A. Harton[11], J.A. Hasenbichler[34], H. Hassan[77], D. Hatzifotiadou[10,53], P. Hauer[42], S. Hayashi[132], A.D.L.B. Hechavarria[144], S.T. Heckel[68], E. Hellbär[68], H. Helstrup[36], A. Herghelegiu[47], E.G. Hernandez[44], G. Herrera Corral[9], F. Herrmann[144], K.F. Hetland[36], T.E. Hilden[43], H. Hillemanns[34], C. Hills[127], B. Hippolyte[136], B. Hohlweger[103], D. Horak[37], S. Hornung[105], R. Hosokawa[16,133], P. Hristov[34], C. Huang[61], C. Hughes[130], P. Huhn[68], T.J. Humanic[95], H. Hushnud[108], L.A. Husova[144], N. Hussain[41], S.A. Hussain[15], D. Hutter[39], D.S. Hwang[19], J.P. Iddon[34,127], R. Ilkaev[107], M. Inaba[133], M. Ippolitov[86], M.S. Islam[108], M. Ivanov[105], V. Ivanov[96], V. Izucheev[89], B. Jacak[78], N. Jacazio[27,53], P.M. Jacobs[78], M.B. Jadhav[48], S. Jadlovska[116], J. Jadlovsky[116], S. Jaelani[63], C. Jahnke[121], M.J. Jakubowska[142], M.A. Janik[142], M. Jercic[97], O. Jevons[109], R.T. Jimenez Bustamante[105], M. Jin[125], F. Jonas[94,144], P.G. Jones[109], A. Jusko[109], P. Kalinak[64], A. Kalweit[34], J.H. Kang[147], V. Kaplin[91], S. Kar[6], A. Karasu Uysal[76], O. Karavichev[62], T. Karavicheva[62], P. Karczmarczyk[34], E. Karpechev[62], U. Kebschull[73], R. Keidel[46], M. Keil[34], B. Ketzer[42], Z. Khabanova[88], A.M. Khan[6], S. Khan[17], S.A. Khan[141], A. Khanzadeev[96], Y. Kharlov[89], A. Khatun[17], A. Khuntia[49,118], B. Kileng[36], B. Kim[60], B. Kim[133], D. Kim[147], D.J. Kim[126], E.J. Kim[13], H. Kim[147], J. Kim[147], J.S. Kim[40], J. Kim[102], J. Kim[147], J. Kim[13], M. Kim[102], S. Kim[19], T. Kim[147], T. Kim[147], S. Kirsch[39], I. Kisel[39], S. Kiselev[90], A. Kisiel[142], J.L. Klay[5], C. Klein[68], J. Klein[58], S. Klein[78], C. Klein-Bösing[144], S. Klewin[102], A. Kluge[34], M.L. Knichel[34], A.G. Knospe[125], C. Kobdaj[115], M.K. Köhler[102], T. Kollegger[105], A. Kondratyev[74], N. Kondratyeva[91], E. Kondratyuk[89], P.J. Konopka[34], L. Koska[116], O. Kovalenko[83], V. Kovalenko[112], M. Kowalski[118], I. Králik[64], A. Kravčáková[38], L. Kreis[105], M. Krivda[64,109], F. Krizek[93], K. Krizkova Gajdosova[37], M. Krüger[68], E. Kryshen[96], M. Krzewicki[39], A.M. Kubera[95], V. Kučera[60], C. Kuhn[136], P.G. Kuijer[88], L. Kumar[98], S. Kumar[48], S. Kundu[84], P. Kurashvili[83], A. Kurepin[62], A.B. Kurepin[62], A. Kuryakin[107], S. Kushpil[93], J. Kvapil[109], M.J. Kweon[60], J.Y. Kwon[60], Y. Kwon[147], S.L. La Pointe[39], P. La Rocca[28], Y.S. Lai[78], R. Langoy[129], K. Lapidus[34,146], A. Lardeux[21], P. Larionov[51], E. Laudi[34], R. Lavicka[37], T. Lazareva[112], R. Lea[25], L. Leardini[102], S. Lee[147], F. Lehas[88], S. Lehner[113], J. Lehrbach[39], R.C. Lemmon[92], I. León Monzón[120], E.D. Lesser[20], M. Lettrich[34], P. Lévai[145], X. Li[12], X.L. Li[6], J. Lien[129], R. Lietava[109], B. Lim[18], S. Lindal[21], V. Lindenstruth[39], S.W. Lindsay[127], C. Lippmann[105], M.A. Lisa[95], V. Litichevskyi[43], A. Liu[78], S. Liu[95], W.J. Llope[143], I.M. Lofnes[22], V. Loginov[91], C. Loizides[94], P. Loncar[35], X. Lopez[134], E. López Torres[8], P. Luettig[68], J.R. Luhder[144], M. Lunardon[29], G. Luparello[59], A. Maevskaya[62], M. Mager[34], S.M. Mahmood[21], T. Mahmoud[42], A. Maire[136], R.D. Majka[146], M. Malaev[96], Q.W. Malik[21], L. Malinina[74, iii], D. Mal'Kevich[90], P. Malzacher[105], G. Mandaglio[55], V. Manko[86], F. Manso[134], V. Manzari[52], Y. Mao[6], M. Marchisone[135], J. Mareš[66], G.V. Margagliotti[25], A. Margotti[53], J. Margutti[63], A. Marín[105], C. Markert[119], M. Marquard[68], N.A. Martin[102], P. Martinengo[34], J.L. Martinez[125],

JHEP02(2020)041

M.I. Martínez[44], G. Martínez García[114], M. Martinez Pedreira[34], S. Masciocchi[105], M. Masera[26], A. Masoni[54], L. Massacrier[61], E. Masson[114], A. Mastroserio[52,138], A.M. Mathis[103,117], O. Matonoha[79], P.F.T. Matuoka[121], A. Matyja[118], C. Mayer[118], M. Mazzilli[33], M.A. Mazzoni[57], A.F. Mechler[68], F. Meddi[23], Y. Melikyan[62,91], A. Menchaca-Rocha[71], C. Mengke[6], E. Meninno[30], M. Meres[14], S. Mhlanga[124], Y. Miake[133], L. Micheletti[26], M.M. Mieskolainen[43], D.L. Mihaylov[103], K. Mikhaylov[74,90], A. Mischke[63, i], A.N. Mishra[69], D. Miśkowiec[105], C.M. Mitu[67], A. Modak[3], N. Mohammadi[34], A.P. Mohanty[63], B. Mohanty[84], M. Mohisin Khan[17, iv], M. Mondal[141], C. Mordasini[103], D.A. Moreira De Godoy[144], L.A.P. Moreno[44], S. Moretto[29], A. Morreale[114], A. Morsch[34], T. Mrnjavac[34], V. Muccifora[51], E. Mudnic[35], D. Mühlheim[144], S. Muhuri[141], J.D. Mulligan[78], M.G. Munhoz[121], K. Münning[42], R.H. Munzer[68], H. Murakami[132], S. Murray[124], L. Musa[34], J. Musinsky[64], C.J. Myers[125], J.W. Myrcha[142], B. Naik[48], R. Nair[83], B.K. Nandi[48], R. Nania[10,53], E. Nappi[52], M.U. Naru[15], A.F. Nassirpour[79], H. Natal da Luz[121], C. Nattrass[130], R. Nayak[48], T.K. Nayak[84,141], S. Nazarenko[107], A. Neagu[21], R.A. Negrao De Oliveira[68], L. Nellen[69], S.V. Nesbo[36], G. Neskovic[39], D. Nesterov[112], B.S. Nielsen[87], S. Nikolaev[86], S. Nikulin[86], V. Nikulin[96], F. Noferini[10,53], P. Nomokonov[74], G. Nooren[63], J. Norman[77], N. Novitzky[133], P. Nowakowski[142], A. Nyanin[86], J. Nystrand[22], M. Ogino[80], A. Ohlson[102], J. Oleniacz[142], A.C. Oliveira Da Silva[121], M.H. Oliver[146], C. Oppedisano[58], R. Orava[43], A. Ortiz Velasquez[69], A. Oskarsson[79], J. Otwinowski[118], K. Oyama[80], Y. Pachmayer[102], V. Pacik[87], D. Pagano[140], G. Paić[69], P. Palni[6], J. Pan[143], A.K. Pandey[48], S. Panebianco[137], P. Pareek[49], J. Park[60], J.E. Parkkila[126], S. Parmar[98], S.P. Pathak[125], R.N. Patra[141], B. Paul[24,58], H. Pei[6], T. Peitzmann[63], X. Peng[6], L.G. Pereira[70], H. Pereira Da Costa[137], D. Peresunko[86], G.M. Perez[8], E. Perez Lezama[68], V. Peskov[68], Y. Pestov[4], V. Petráček[37], M. Petrovici[47], R.P. Pezzi[70], S. Piano[59], M. Pikna[14], P. Pillot[114], L.O.D.L. Pimentel[87], O. Pinazza[34,53], L. Pinsky[125], C. Pinto[28], S. Pisano[51], D. Pistone[55], D.B. Piyarathna[125], M. Płoskoń[78], M. Planinic[97], F. Pliquett[68], J. Pluta[142], S. Pochybova[145], M.G. Poghosyan[94], B. Polichtchouk[89], N. Poljak[97], A. Pop[47], H. Poppenborg[144], S. Porteboeuf-Houssais[134], V. Pozdniakov[74], S.K. Prasad[3], R. Preghenella[53], F. Prino[58], C.A. Pruneau[143], I. Pshenichnov[62], M. Puccio[26,34], V. Punin[107], K. Puranapanda[141], J. Putschke[143], R.E. Quishpe[125], S. Ragoni[109], S. Raha[3], S. Rajput[99], J. Rak[126], A. Rakotozafindrabe[137], L. Ramello[32], F. Rami[136], R. Raniwala[100], S. Raniwala[100], S.S. Räsänen[43], B.T. Rascanu[68], R. Rath[49], V. Ratza[42], I. Ravasenga[31], K.F. Read[94,130], K. Redlich[83, v], A. Rehman[22], P. Reichelt[68], F. Reidt[34], X. Ren[6], R. Renfordt[68], A. Reshetin[62], J.-P. Revol[10], K. Reygers[102], V. Riabov[96], T. Richert[79,87], M. Richter[21], P. Riedler[34], W. Riegler[34], F. Riggi[28], C. Ristea[67], S.P. Rode[49], M. Rodríguez Cahuantzi[44], K. Røed[21], R. Rogalev[89], E. Rogochaya[74], D. Rohr[34], D. Röhrich[22], P.S. Rokita[142], F. Ronchetti[51], E.D. Rosas[69], K. Roslon[142], P. Rosnet[134], A. Rossi[29], A. Rotondi[139], F. Roukoutakis[82], A. Roy[49], P. Roy[108], O.V. Rueda[79], R. Rui[25], B. Rumyantsev[74], A. Rustamov[85], E. Ryabinkin[86], Y. Ryabov[96], A. Rybicki[118], H. Rytkonen[126], S. Sadhu[141], S. Sadovsky[89], K. Šafařík[34,37], S.K. Saha[141], B. Sahoo[48], P. Sahoo[48,49], R. Sahoo[49], S. Sahoo[65], P.K. Sahu[65], J. Saini[141], S. Sakai[133], S. Sambyal[99], V. Samsonov[91,96], F.R. Sanchez[44], A. Sandoval[71], A. Sarkar[72], D. Sarkar[143], N. Sarkar[141], P. Sarma[41], V.M. Sarti[103], M.H.P. Sas[63], E. Scapparone[53], B. Schaefer[94], J. Schambach[119], H.S. Scheid[68], C. Schiaua[47], R. Schicker[102], A. Schmah[102], C. Schmidt[105], H.R. Schmidt[101], M.O. Schmidt[102], M. Schmidt[101], N.V. Schmidt[68,94], A.R. Schmier[130], J. Schukraft[34,87], Y. Schutz[34,136], K. Schwarz[105], K. Schweda[105], G. Scioli[27], E. Scomparin[58], M. Šefčík[38], J.E. Seger[16], Y. Sekiguchi[132], D. Sekihata[45,132], I. Selyuzhenkov[91,105], S. Senyukov[136], D. Serebryakov[62], E. Serradilla[71], P. Sett[48], A. Sevcenco[67], A. Shabanov[62], A. Shabetai[114], R. Shahoyan[34], W. Shaikh[108], A. Shangaraev[89], A. Sharma[98], A. Sharma[99], H. Sharma[118], M. Sharma[99], N. Sharma[98], A.I. Sheikh[141], K. Shigaki[45], M. Shimomura[81], S. Shirinkin[90], Q. Shou[111], Y. Sibiriak[86], S. Siddhanta[54], T. Siemiarczuk[83],

JHEP02(2020)041

D. Silvermyr[79], C. Silvestre[77], G. Simatovic[88], G. Simonetti[34,103], R. Singh[84], R. Singh[99], V.K. Singh[141], V. Singhal[141], T. Sinha[108], B. Sitar[14], M. Sitta[32], T.B. Skaali[21], M. Slupecki[126], N. Smirnov[146], R.J.M. Snellings[63], T.W. Snellman[43,126], J. Sochan[116], C. Soncco[110], J. Song[60,125], A. Songmoolnak[115], F. Soramel[29], S. Sorensen[130], I. Sputowska[118], J. Stachel[102], I. Stan[67], P. Stankus[94], P.J. Steffanic[130], E. Stenlund[79], D. Stocco[114], M.M. Storetvedt[36], P. Strmen[14], A.A.P. Suaide[121], T. Sugitate[45], C. Suire[61], M. Suleymanov[15], M. Suljic[34], R. Sultanov[90], M. Šumbera[93], S. Sumowidagdo[50], K. Suzuki[113], S. Swain[65], A. Szabo[14], I. Szarka[14], U. Tabassam[15], G. Taillepied[134], J. Takahashi[122], G.J. Tambave[22], S. Tang[6,134], M. Tarhini[114], M.G. Tarzila[47], A. Tauro[34], G. Tejeda Muñoz[44], A. Telesca[34], C. Terrevoli[29,125], D. Thakur[49], S. Thakur[141], D. Thomas[119], F. Thoresen[87], R. Tieulent[135], A. Tikhonov[62], A.R. Timmins[125], A. Toia[68], N. Topilskaya[62], M. Toppi[51], F. Torales-Acosta[20], S.R. Torres[120], A. Trifiro[55], S. Tripathy[49], T. Tripathy[48], S. Trogolo[29], G. Trombetta[33], L. Tropp[38], V. Trubnikov[2], W.H. Trzaska[126], T.P. Trzcinski[142], B.A. Trzeciak[63], T. Tsuji[132], A. Tumkin[107], R. Turrisi[56], T.S. Tveter[21], K. Ullaland[22], E.N. Umaka[125], A. Uras[135], G.L. Usai[24], A. Utrobicic[97], M. Vala[38,116], N. Valle[139], S. Vallero[58], N. van der Kolk[63], L.V.R. van Doremalen[63], M. van Leeuwen[63], P. Vande Vyvre[34], D. Varga[145], Z. Varga[145], M. Varga-Kofarago[145], A. Vargas[44], M. Vargyas[126], R. Varma[48], M. Vasileiou[82], A. Vasiliev[86], O. Vázquez Doce[103,117], V. Vechernin[112], A.M. Veen[63], E. Vercellin[26], S. Vergara Limón[44], L. Vermunt[63], R. Vernet[7], R. Vértesi[145], M.G.D.L.C. Vicencio[9], L. Vickovic[35], J. Viinikainen[126], Z. Vilakazi[131], O. Villalobos Baillie[109], A. Villatoro Tello[44], G. Vino[52], A. Vinogradov[86], T. Virgili[30], V. Vislavicius[87], A. Vodopyanov[74], B. Volkel[34], M.A. Völkl[101], K. Voloshin[90], S.A. Voloshin[143], G. Volpe[33], B. von Haller[34], I. Vorobyev[103], D. Voscek[116], J. Vrláková[38], B. Wagner[22], M. Weber[113], S.G. Weber[105,144], A. Wegrzynek[34], D.F. Weiser[102], S.C. Wenzel[34], J.P. Wessels[144], E. Widmann[113], J. Wiechula[68], J. Wikne[21], G. Wilk[83], J. Wilkinson[53], G.A. Willems[34], E. Willsher[109], B. Windelband[102], W.E. Witt[130], Y. Wu[128], R. Xu[6], S. Yalcin[76], K. Yamakawa[45], S. Yang[22], S. Yano[137], Z. Yin[6], H. Yokoyama[63,133], I.-K. Yoo[18], J.H. Yoon[60], S. Yuan[22], A. Yuncu[102], V. Yurchenko[2], V. Zaccolo[25,58], A. Zaman[15], C. Zampolli[34], H.J.C. Zanoli[63,121], N. Zardoshti[34], A. Zarochentsev[112], P. Závada[66], N. Zaviyalov[107], H. Zbroszczyk[142], M. Zhalov[96], X. Zhang[6], Z. Zhang[6], C. Zhao[21], V. Zherebchevskii[112], N. Zhigareva[90], D. Zhou[6], Y. Zhou[87], Z. Zhou[22], J. Zhu[6], Y. Zhu[6], A. Zichichi[10,27], M.B. Zimmermann[34], G. Zinovjev[2], N. Zurlo[140],

[1] *Deceased*
[2] *Dipartimento DET del Politecnico di Torino, Turin, Italy*
[3] *M.V. Lomonosov Moscow State University, D.V. Skobeltsyn Institute of Nuclear, Physics, Moscow, Russia*
[4] *Department of Applied Physics, Aligarh Muslim University, Aligarh, India*
[5] *Institute of Theoretical Physics, University of Wroclaw, Poland*

[1] *A.I. Alikhanyan National Science Laboratory (Yerevan Physics Institute) Foundation, Yerevan, Armenia*
[2] *Bogolyubov Institute for Theoretical Physics, National Academy of Sciences of Ukraine, Kiev, Ukraine*
[3] *Bose Institute, Department of Physics and Centre for Astroparticle Physics and Space Science (CAPSS), Kolkata, India*
[4] *Budker Institute for Nuclear Physics, Novosibirsk, Russia*
[5] *California Polytechnic State University, San Luis Obispo, California, United States*
[6] *Central China Normal University, Wuhan, China*
[7] *Centre de Calcul de l'IN2P3, Villeurbanne, Lyon, France*
[8] *Centro de Aplicaciones Tecnológicas y Desarrollo Nuclear (CEADEN), Havana, Cuba*

JHEP02(2020)041

[9] Centro de Investigación y de Estudios Avanzados (CINVESTAV), Mexico City and Mérida, Mexico
[10] Centro Fermi - Museo Storico della Fisica e Centro Studi e Ricerche "Enrico Fermi', Rome, Italy
[11] Chicago State University, Chicago, Illinois, United States
[12] China Institute of Atomic Energy, Beijing, China
[13] Chonbuk National University, Jeonju, Republic of Korea
[14] Comenius University Bratislava, Faculty of Mathematics, Physics and Informatics, Bratislava, Slovakia
[15] COMSATS University Islamabad, Islamabad, Pakistan
[16] Creighton University, Omaha, Nebraska, United States
[17] Department of Physics, Aligarh Muslim University, Aligarh, India
[18] Department of Physics, Pusan National University, Pusan, Republic of Korea
[19] Department of Physics, Sejong University, Seoul, Republic of Korea
[20] Department of Physics, University of California, Berkeley, California, United States
[21] Department of Physics, University of Oslo, Oslo, Norway
[22] Department of Physics and Technology, University of Bergen, Bergen, Norway
[23] Dipartimento di Fisica dell'Università 'La Sapienza' and Sezione INFN, Rome, Italy
[24] Dipartimento di Fisica dell'Università and Sezione INFN, Cagliari, Italy
[25] Dipartimento di Fisica dell'Università and Sezione INFN, Trieste, Italy
[26] Dipartimento di Fisica dell'Università and Sezione INFN, Turin, Italy
[27] Dipartimento di Fisica e Astronomia dell'Università and Sezione INFN, Bologna, Italy
[28] Dipartimento di Fisica e Astronomia dell'Università and Sezione INFN, Catania, Italy
[29] Dipartimento di Fisica e Astronomia dell'Università and Sezione INFN, Padova, Italy
[30] Dipartimento di Fisica 'E.R. Caianiello' dell'Università and Gruppo Collegato INFN, Salerno, Italy
[31] Dipartimento DISAT del Politecnico and Sezione INFN, Turin, Italy
[32] Dipartimento di Scienze e Innovazione Tecnologica dell'Università del Piemonte Orientale and INFN Sezione di Torino, Alessandria, Italy
[33] Dipartimento Interateneo di Fisica 'M. Merlin' and Sezione INFN, Bari, Italy
[34] European Organization for Nuclear Research (CERN), Geneva, Switzerland
[35] Faculty of Electrical Engineering, Mechanical Engineering and Naval Architecture, University of Split, Split, Croatia
[36] Faculty of Engineering and Science, Western Norway University of Applied Sciences, Bergen, Norway
[37] Faculty of Nuclear Sciences and Physical Engineering, Czech Technical University in Prague, Prague, Czech Republic
[38] Faculty of Science, P.J. Šafárik University, Košice, Slovakia
[39] Frankfurt Institute for Advanced Studies, Johann Wolfgang Goethe-Universität Frankfurt, Frankfurt, Germany
[40] Gangneung-Wonju National University, Gangneung, Republic of Korea
[41] Gauhati University, Department of Physics, Guwahati, India
[42] Helmholtz-Institut für Strahlen- und Kernphysik, Rheinische Friedrich-Wilhelms-Universität Bonn, Bonn, Germany
[43] Helsinki Institute of Physics (HIP), Helsinki, Finland
[44] High Energy Physics Group, Universidad Autónoma de Puebla, Puebla, Mexico
[45] Hiroshima University, Hiroshima, Japan
[46] Hochschule Worms, Zentrum für Technologietransfer und Telekommunikation (ZTT), Worms, Germany
[47] Horia Hulubei National Institute of Physics and Nuclear Engineering, Bucharest, Romania
[48] Indian Institute of Technology Bombay (IIT), Mumbai, India
[49] Indian Institute of Technology Indore, Indore, India
[50] Indonesian Institute of Sciences, Jakarta, Indonesia
[51] INFN, Laboratori Nazionali di Frascati, Frascati, Italy
[52] INFN, Sezione di Bari, Bari, Italy

JHEP02(2020)041

[53] *INFN, Sezione di Bologna, Bologna, Italy*
[54] *INFN, Sezione di Cagliari, Cagliari, Italy*
[55] *INFN, Sezione di Catania, Catania, Italy*
[56] *INFN, Sezione di Padova, Padova, Italy*
[57] *INFN, Sezione di Roma, Rome, Italy*
[58] *INFN, Sezione di Torino, Turin, Italy*
[59] *INFN, Sezione di Trieste, Trieste, Italy*
[60] *Inha University, Incheon, Republic of Korea*
[61] *Institut de Physique Nucléaire d'Orsay (IPNO), Institut National de Physique Nucléaire et de Physique des Particules (IN2P3/CNRS), Université de Paris-Sud, Université Paris-Saclay, Orsay, France*
[62] *Institute for Nuclear Research, Academy of Sciences, Moscow, Russia*
[63] *Institute for Subatomic Physics, Utrecht University/Nikhef, Utrecht, Netherlands*
[64] *Institute of Experimental Physics, Slovak Academy of Sciences, Košice, Slovakia*
[65] *Institute of Physics, Homi Bhabha National Institute, Bhubaneswar, India*
[66] *Institute of Physics of the Czech Academy of Sciences, Prague, Czech Republic*
[67] *Institute of Space Science (ISS), Bucharest, Romania*
[68] *Institut für Kernphysik, Johann Wolfgang Goethe-Universität Frankfurt, Frankfurt, Germany*
[69] *Instituto de Ciencias Nucleares, Universidad Nacional Autónoma de México, Mexico City, Mexico*
[70] *Instituto de Física, Universidade Federal do Rio Grande do Sul (UFRGS), Porto Alegre, Brazil*
[71] *Instituto de Física, Universidad Nacional Autónoma de México, Mexico City, Mexico*
[72] *iThemba LABS, National Research Foundation, Somerset West, South Africa*
[73] *Johann-Wolfgang-Goethe Universität Frankfurt Institut für Informatik, Fachbereich Informatik und Mathematik, Frankfurt, Germany*
[74] *Joint Institute for Nuclear Research (JINR), Dubna, Russia*
[75] *Korea Institute of Science and Technology Information, Daejeon, Republic of Korea*
[76] *KTO Karatay University, Konya, Turkey*
[77] *Laboratoire de Physique Subatomique et de Cosmologie, Université Grenoble-Alpes, CNRS-IN2P3, Grenoble, France*
[78] *Lawrence Berkeley National Laboratory, Berkeley, California, United States*
[79] *Lund University Department of Physics, Division of Particle Physics, Lund, Sweden*
[80] *Nagasaki Institute of Applied Science, Nagasaki, Japan*
[81] *Nara Women's University (NWU), Nara, Japan*
[82] *National and Kapodistrian University of Athens, School of Science, Department of Physics , Athens, Greece*
[83] *National Centre for Nuclear Research, Warsaw, Poland*
[84] *National Institute of Science Education and Research, Homi Bhabha National Institute, Jatni, India*
[85] *National Nuclear Research Center, Baku, Azerbaijan*
[86] *National Research Centre Kurchatov Institute, Moscow, Russia*
[87] *Niels Bohr Institute, University of Copenhagen, Copenhagen, Denmark*
[88] *Nikhef, National institute for subatomic physics, Amsterdam, Netherlands*
[89] *NRC Kurchatov Institute IHEP, Protvino, Russia*
[90] *NRC Kurchatov Institute - ITEP, Moscow, Russia*
[91] *NRNU Moscow Engineering Physics Institute, Moscow, Russia*
[92] *Nuclear Physics Group, STFC Daresbury Laboratory, Daresbury, United Kingdom*
[93] *Nuclear Physics Institute of the Czech Academy of Sciences, Řež u Prahy, Czech Republic*
[94] *Oak Ridge National Laboratory, Oak Ridge, Tennessee, United States*
[95] *Ohio State University, Columbus, Ohio, United States*
[96] *Petersburg Nuclear Physics Institute, Gatchina, Russia*
[97] *Physics department, Faculty of science, University of Zagreb, Zagreb, Croatia*
[98] *Physics Department, Panjab University, Chandigarh, India*
[99] *Physics Department, University of Jammu, Jammu, India*

JHEP02(2020)041

[100] Physics Department, University of Rajasthan, Jaipur, India
[101] Physikalisches Institut, Eberhard-Karls-Universität Tübingen, Tübingen, Germany
[102] Physikalisches Institut, Ruprecht-Karls-Universität Heidelberg, Heidelberg, Germany
[103] Physik Department, Technische Universität München, Munich, Germany
[104] Politecnico di Bari, Bari, Italy
[105] Research Division and ExtreMe Matter Institute EMMI, GSI Helmholtzzentrum für Schwerionenforschung GmbH, Darmstadt, Germany
[106] Rudjer Bošković Institute, Zagreb, Croatia
[107] Russian Federal Nuclear Center (VNIIEF), Sarov, Russia
[108] Saha Institute of Nuclear Physics, Homi Bhabha National Institute, Kolkata, India
[109] School of Physics and Astronomy, University of Birmingham, Birmingham, United Kingdom
[110] Sección Física, Departamento de Ciencias, Pontificia Universidad Católica del Perú, Lima, Peru
[111] Shanghai Institute of Applied Physics, Shanghai, China
[112] St. Petersburg State University, St. Petersburg, Russia
[113] Stefan Meyer Institut für Subatomare Physik (SMI), Vienna, Austria
[114] SUBATECH, IMT Atlantique, Université de Nantes, CNRS-IN2P3, Nantes, France
[115] Suranaree University of Technology, Nakhon Ratchasima, Thailand
[116] Technical University of Košice, Košice, Slovakia
[117] Technische Universität München, Excellence Cluster 'Universe', Munich, Germany
[118] The Henryk Niewodniczanski Institute of Nuclear Physics, Polish Academy of Sciences, Cracow, Poland
[119] The University of Texas at Austin, Austin, Texas, United States
[120] Universidad Autónoma de Sinaloa, Culiacán, Mexico
[121] Universidade de São Paulo (USP), São Paulo, Brazil
[122] Universidade Estadual de Campinas (UNICAMP), Campinas, Brazil
[123] Universidade Federal do ABC, Santo Andre, Brazil
[124] University of Cape Town, Cape Town, South Africa
[125] University of Houston, Houston, Texas, United States
[126] University of Jyväskylä, Jyväskylä, Finland
[127] University of Liverpool, Liverpool, United Kingdom
[128] University of Science and Techonology of China, Hefei, China
[129] University of South-Eastern Norway, Tonsberg, Norway
[130] University of Tennessee, Knoxville, Tennessee, United States
[131] University of the Witwatersrand, Johannesburg, South Africa
[132] University of Tokyo, Tokyo, Japan
[133] University of Tsukuba, Tsukuba, Japan
[134] Université Clermont Auvergne, CNRS/IN2P3, LPC, Clermont-Ferrand, France
[135] Université de Lyon, Université Lyon 1, CNRS/IN2P3, IPN-Lyon, Villeurbanne, Lyon, France
[136] Université de Strasbourg, CNRS, IPHC UMR 7178, F-67000 Strasbourg, France, Strasbourg, France
[137] Université Paris-Saclay Centre d'Etudes de Saclay (CEA), IRFU, Départment de Physique Nucléaire (DPhN), Saclay, France
[138] Università degli Studi di Foggia, Foggia, Italy
[139] Università degli Studi di Pavia, Pavia, Italy
[140] Università di Brescia, Brescia, Italy
[141] Variable Energy Cyclotron Centre, Homi Bhabha National Institute, Kolkata, India
[142] Warsaw University of Technology, Warsaw, Poland
[143] Wayne State University, Detroit, Michigan, United States
[144] Westfälische Wilhelms-Universität Münster, Institut für Kernphysik, Münster, Germany
[145] Wigner Research Centre for Physics, Hungarian Academy of Sciences, Budapest, Hungary
[146] Yale University, New Haven, Connecticut, United States
[147] Yonsei University, Seoul, Republic of Korea

JHEP02(2020)041